Friction

Review Article

A review of drag reduction methods and principles in bionic interface

Yiwei Hu, Yukai Sun, Liran Ma, Jianbin Luo✉

Cite this article: Hu YW, Sun YK, Ma LR, et al. *Friction* 2025, **13**(9): 9441033. https://doi.org/10.26599/FRICT.2025.9441033

ABSTRACT: Natural organisms have evolved numerous functional surfaces and structures on their body surfaces over billions of years of evolution, which have shown excellent drag reduction effects in a wide range of applications. From a biomimicry perspective, techniques for reducing drag, such as compliant walls, superhydrophobic surfaces, and surface textures, originate from the features of living things in the natural world. These techniques, which are important for sustainable development, can increase productivity, cut down on energy loss, preserve the environment, and be applied to industrial production, sports, transportation, and other areas. This paper presents systematic elaboration of the structure or properties of functional surfaces from the standpoint of typical biological characteristics. Additionally, a summary of bionic drag reduction techniques, guiding principles, and related research findings is provided, which can serve as a resource for both further study and real-world implementation.

KEYWORDS: biomimicry; drag reduction; surface texture; superhydrophobic; compliant walls; polymers

1 Introduction

The field of bionics examines the composition and mechanisms of living things. It uses this knowledge to solve scientific and engineering issues, which is becoming increasingly popular as science and technology continue to advance. Bionic interface drag reduction technology has garnered significant interest across various domains because of its extensive development potential and broad range of applications [1–3]. Through billions of years of evolution, naturally occurring organisms have developed a variety of distinctive structures and abilities that allow them to adapt to their surroundings. Among them, many biological body surfaces—such as the skin of sharks—have exceptional drag-reducing qualities [4, 5]. Owing to their unique surface morphology, microstructure, or material properties, these organisms improve their movement efficiency and decrease their resistance in fluids. The development of bionic interface drag reduction technology has been influenced by these organisms [4, 6–11]. According to the data, frictional resistance makes up roughly half of all resistance in aircraft [11]. Approximately 80% of the resistance of low-speed ships is frictional. In the case of pipeline transportation, the figure is at least 95% [8, 9, 12–16]. In addition, underwater vehicles such as submarines can achieve a 3%–7% increase in speed and range if the resistance is lowered by approximately 10% in comparison with standard navigation [6, 17, 18]. As a result, decreasing fluid resistance enhances the effectiveness of movement, safeguards the environment, and fosters economic growth [19–26].

This paper presents biological structures with excellent drag reduction properties in four sections: surface textures, compliant walls, superhydrophobic surfaces, and polymer additives. The functional traits, morphological features, and research focus of the corresponding organisms are discussed, along with the corresponding drag reduction mechanisms. Guidance and recommendations are given for the practical application of bionic surfaces by summarizing, contrasting, and prospecting the bionic drag reduction techniques.

2 Surface texture

This section focuses on the drag reduction method of preparing functional surfaces modeled after biological surface texture. Biological prototypes include sharks, shrimp, loaches, grass carp, puffer fish, crocodiles, and dung beetles. Biological surfaces have both macrostructures and microstructures, which are summarized and outlined in terms of their structural characteristics, research content, and drag reduction principles.

2.1 Shark

2.1.1 Shape characteristics and research content

Sharks, as the top predator of the ocean and one of the fishes with the longest evolutionary history [27], have excellent locomotor abilities in water. To catch prey, its speed can reach 60 km/h [6]. Scientists have been intrigued by the paradox of how sharks, despite their large size, which can create resistance, can accelerate

State Key Laboratory of Tribology in Advanced Equipment, Tsinghua University, Beijing 100084, China.

✉ Corresponding author. E-mail: luojb@tsinghua.edu.cn

Received: June 12, 2024; Revised: September 24, 2024; Accepted: November 4, 2024

and steer with outstanding ability [4]. Thus, the surface structure of sharks has been analyzed and studied. An analysis of the surface structure of various shark species has revealed that the surface of most sharks is not smooth but consists of different denticle structures that are interlaced with each other [28]. In addition, these denticles differ in various parts of the same shark, such as the head and tail, as well as in the same part of different species of shark [29–31]. This difference is closely related to the fact that each part of the shark faces different flow separation and turbulence, as well as to the fact that different sharks have different body sizes, speeds of locomotion and acceleration capabilities. The shark denticle structure is shown in Figs. 1(a) and 1(b). Moreover, the shark epidermis is relatively soft, and the denticle structure is embedded in the dermis. This structure allows the surface riblet structure of sharks to be tilted and varied [32, 33], which enables the shark to adaptively reduce drag in different directions of advancement, thus reducing unnecessary energy loss. The denticle structure has two layers, an outer layer of enamel and an inner layer of skeletal structure, which together form an elaborate three-dimensional (3D) system [34], facilitating the rapid movement of sharks in the water.

The drag reduction effect of denticle structure is verified via experiments and simulations. In 2008, Han et al. [38] achieved low-cost fabrication of bionic surfaces with better accuracy and higher efficiency by the hot pressing method. Their method replicated the shark surface and they then tested it in a water hole, and the highest drag reduction rate of 8.25% was obtained. After that, Zhang et al. [39] tested the scanned shark epidermal model as well as the real structure obtained by biological replication utilizing a combination of simulation and experimentation and obtained a drag reduction rate of up to 9.55% in the experiment and a drag reduction rate of nearly 14% in the simulation. Wen et al. [35] imitated a real shark denticle structure and elastic surface by computed tomography (CT) scanning technique and 3D printing, as shown in Figs. 1(c) and 1(d). The bionic surface was found to exhibit a drag reduction rate of 8.7% at slow water velocities, while the surface was found to reduce energy consumption by 5.9% through a robotic paddling motion.

However, not all experiments or simulations have yielded the desired drag reduction. Boomsma and Sotiropoulos [40] simulated both uniform and staggered rows of denticle structures by direct numerical simulation and also simulated U-shaped ribs to validate the method. Finally, both shark-like structures increased the drag force by 44% and 50%,while the ribs had a drag reduction effect of 5.2%. In the same year, Pu et al. [41] prepared a shark skin imitation surface by the polydimethylsiloxane elastomer stamping method and obtained an approximately 12% drag reduction by revolution per minute (RPM) torque curve analysis. Ibrahim et al. [42] investigated the drag reduction effect of imitation sharkskin on a real hull model by simulation and found that the friction coefficient was reduced by 3.75%, while the drag was reduced by 3.89% by comparing the turbulence data. In addition to studies that use water as a medium, tests have also been conducted on imitation shark skin in the air. Afterwards, Bhatia et al. [43] tested the aerodynamic drag reduction effect and lift enhancement of shark skin denticles by simulations and obtained a drag reduction rate of 4.3%.

The above research on drag reduction in imitation shark skin structures revealed that different experimental conditions and methods, testing media, and precision of the manufacturing method can affect the actual drag reduction effect or even increase drag. Moreover, as mentioned previously, the diversity, flexibility, and mobility of the shark skin structure present challenges for the study of drag reduction in imitation shark skin. Combining multiple factors to produce a better linkage effect is the key to improving the ability of various types of shark skin-like structures. Moreover, we need to further explore the drag reduction principle of shark skin to guide the design of shark-like skin structures.

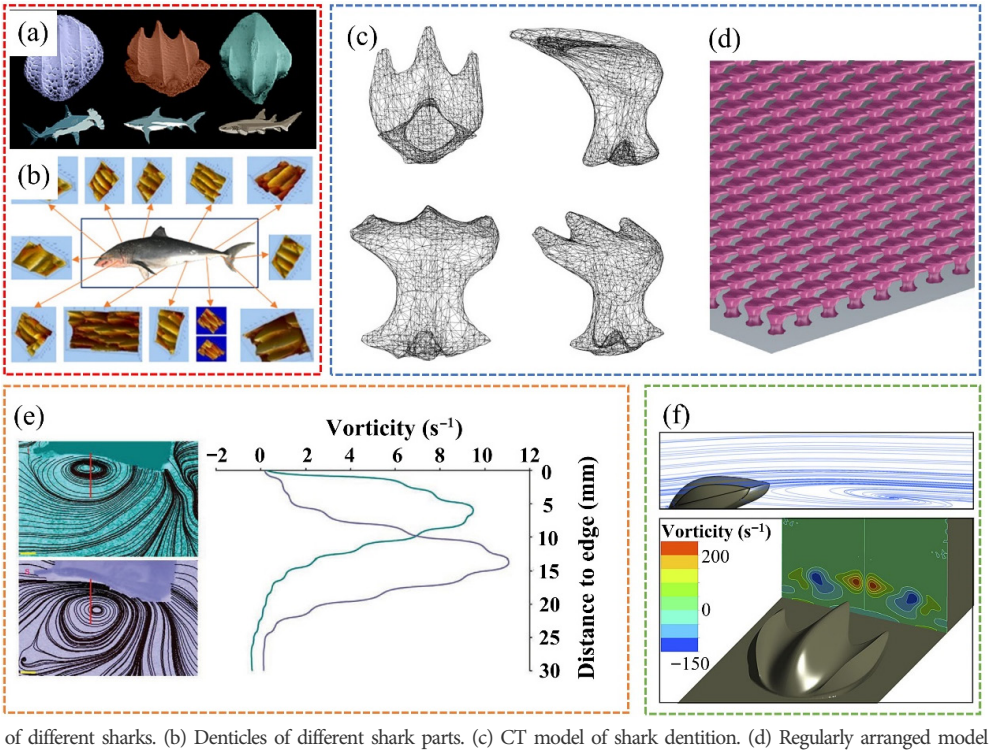

Fig. 1 (a) Denticles of different sharks. (b) Denticles of different shark parts. (c) CT model of shark dentition. (d) Regularly arranged model of a shark denticle. (e) Comparison of vortex morphology and distances between intact shark epidermal structures with flat bands and polished epidermal structures. (f) Simulation analysis of shark denticle structures. Reproduced with permission from Ref. [6] for (a), © Elsevier, 2023; from Ref. [35] for (b–d), © The Company of Biologists Ltd. 2014; from Ref. [36] for (e), © The Company of Biologists Ltd. 2012; from Ref. [37] for (f), © The Author(s) 2018.

2.1.2 Drag reduction principles

The actual shark epidermal structure is more complex and varied, which makes investigating the drag reduction principle of the shark denticle structure more challenging. Moreover, the expansion and contraction of the shark denticle structure in response to water flow also greatly increases the research difficulty. Therefore, there is no universal theory on drag reduction in real shark structures. However, several experimental and simulation studies have been conducted. With respect to the swimming of sharks in water, at the beginning of the 21st century, Wilga and Lauder [44, 45] investigated the hydrodynamic effect of sharks during swimming and found that there was flow separation in the tails of sharks; this phenomenon prompted the subsequent investigation of the drag reduction principle of shark denticle epidermal structure. Then, Lang et al. [46] conducted experiments on the vertical shark denticle structure in a water hole, showing the vortex structure by the fluorescence staining technique, and at the same time studied the vortex and boundary layer state by electron particle image velocimetry. The results showed that the erected denticle structure may be able to control separation and delay the transition from laminar to turbulent flow. Oeffner and Lauder [36] used electron particle velocimetry to observe the flow characteristics of a structure covered with sharkskin as well as a polished, non-toothed surface, and the experiment yielded a 12.3% drag reduction in 2021. Oeffner and Lauder [36] argued that the denticle structure allowed the leading-edge vortices to be closer to the epidermis, and the vortex was the region of lower pressure; at the same time, the center of the vortex was the region of lowest pressure. Thus, the distance of the vortex influences the differential pressure force, which affects the drag reduction effect and the acceleration of the shark, and the vortex situation is shown in Fig. 1(e). In addition, Wen et al. [35] analyzed the flow field and verified the results of Oeffner and Lauder [36] and found the same flow field structure by experiments. In the same year, Lang et al. [48] explored the ability of the surface denticle structure of sharks to influence flow separation through water hole experiments. they found that the return flow would be hindered by the denticle structure, thus affecting the fluid structure, and believed that this ability could explain the drag reduction effect of the denticle structure to a certain extent. Wen et al. [49] again used 3D printing to fabricate composite epidermal structures with soft substrates and hard denticle structures. Static and dynamic studies in a water hole explored the effect of the arrangement of shark-like epidermal microstructures on drag reduction effectiveness or kinematics and found that interlocking and overlapping structures had the best structure, illustrating the effectiveness of the arrangement of dentate structures on shark surfaces. After several years, Domel et al. [37] explored the use of shark-like epidermal microstructures on spacecraft through a combination of experiments and simulations and summarized two principles of drag reduction: on one hand, the denticle structure can control the boundary layer of contact and form separation bubbles, which change the fluid structure of the boundary; on the other hand, the spreading non-horizontal structure creates a vortex along the flow direction, and this vortex contributes to drag reduction, as shown in Fig. 1(f). Patricia et al. [50] investigated the drag reduction performance of three different shapes of shark denticles via simulation and reported that shape has a large effect, suggesting that the variability of shark denticles is justified under different flow conditions. Moreover, it was concluded that the prominent denticle structure reduced the flow separation. Guo et al. [51] constructed a scanned shark epidermal model by 3D printing, conducted experiments in a towing pool, and, combined with data from particle velocimetry, found that dynamic conditions and small-scale perturbations can mitigate boundary layer separation through transient corrections to the local pressure-gradient distributions, which means that it is possible to influence the flow conditions in the boundary layer.

Summarizing the above studies and existing theories, a simple statement on the drag reduction principle of the denticle structure is made. The denticle structure can decrease the distance between the critical vortex and the surface skin, which affects the flow field region at the boundary. Moreover, the surface denticle structure reduces the effect of flow separation and delays the transition of the boundary layer, and the delay in transition helps to reduce drag. These effects on the flow field act in the vicinity of the shark epidermis, resulting in reduced drag on the shark surface, which facilitates the rapid movement of the shark through the water. For more in-depth principles, further research is needed.

2.2 Simplified structure inspired by sharks

2.2.1 Shape characteristics and research content

Inspired by the denticle structure on the surface of sharks, different types of riblet structures have been developed [4, 8, 52]. These riblet structures have been tested in various experiments and simulations [53–60], and different drag reduction or drag enhancement effects have been obtained. In addition, for the wing feathers of some birds, researchers have found riblet microstructures through microscopic observation, and these structures have been found to have the same drag reduction effect [61]. For example, Chen et al. [62, 63] investigated the feathers of various birds. Compared with traditional riblets, the drag reduction rate of herringbone riblets can reach 15%. Overall, the riblet structures are mainly of these types, as shown in Fig. 2(a), including V-shaped grooves, U-shaped grooves, and moment-shaped grooves.

The earliest experimental study of the drag reduction properties of grooves was conducted by Walsh and colleagues at the NASA Research Center. In the late 1970s and early 1980s, they investigated several types of grooves and their drag reduction effects under different experimental conditions [62–68]. Subsequently, more related studies began to develop, such as the studies of Quass et al. [69] and Gallagher and Thomas [70]. In 1990, Walsh summarized the studies on riblets and explained the factors affecting the drag reduction effect of riblets and the related experimental conditions [57, 71], in which the expressions for the two dimensionless parameters, s^+ and h^+, are shown in Eqs. (1) and (2). The meanings of s and h are shown in Fig. 2(b).

$$h^+ = (hu_\infty/\nu)\sqrt{c_f/2} \tag{1}$$

$$s^+ = (su_\infty/\nu)\sqrt{c_f/2} \tag{2}$$

where h is the height of the shape; s is the spacing of the shape; u_∞ represents the external flow field velocity; c_f represents the friction coefficient, which can be approximated by the Reynolds number. This study reveals that the drag reduction effect exists when h^+ is within 25 and s^+ is within 30, and the maximum drag reduction rate occurs when the values of s^+ and h^+ are approximately 12. Later, with the development of computational techniques, the principle theory of drag reduction in riblet structures became clearer, such as the work of Bacher and Smith [72], Weiss [73], Bechert et al. [74], and others; some elements include the analysis of turbulence phenomena as well as the explanation of secondary vortices. Garcia et al. [75] proposed another dimensionless

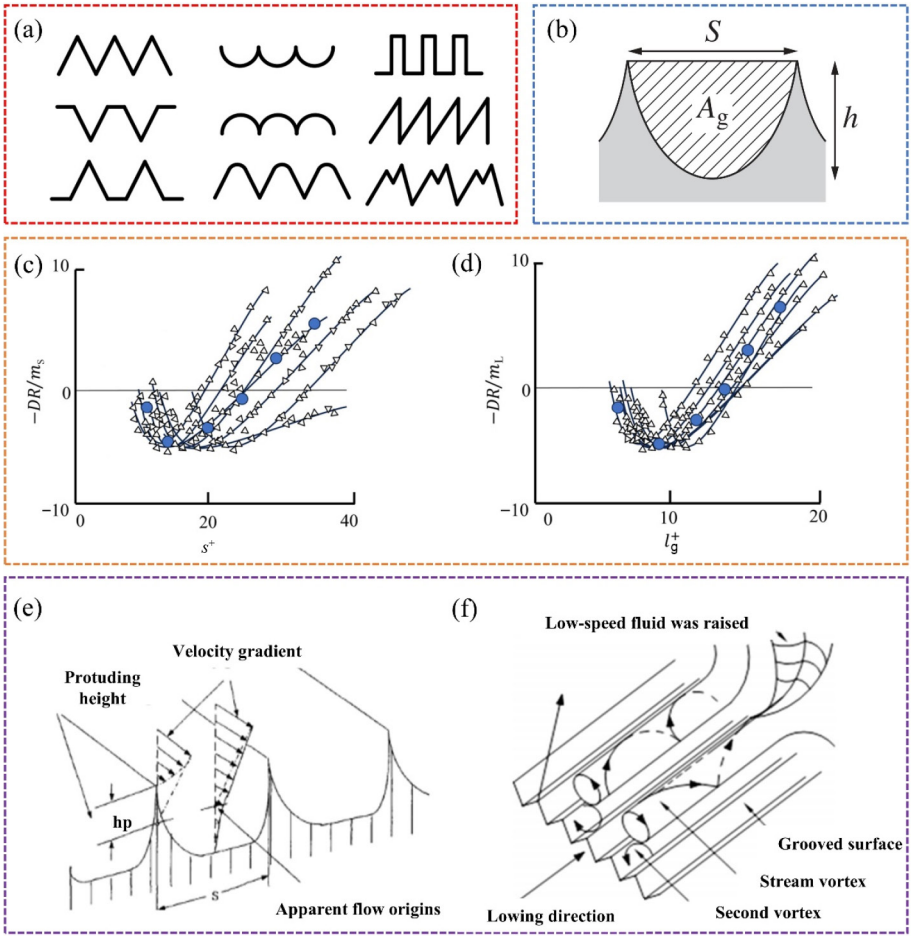

Fig. 2 (a) Various shapes of riblets. (b) Cross section of riblet, where S represents width; H represents height; A_g represents area of flow. (c) Drag reduction as a function of spacing s^+. (d) Drag reduction as a function of square root of groove cross-section l_g^+. (e) Schematic of protruding height theory. (f) Schematic of secondary vortex theory. Reproduced with permission from Ref. [5], © World Scientific Publishing Company 2015.

parameter l^+ in 2011 by analyzing the experimental and simulation data of their predecessors, which is shown in Eq. (3).

$$l^+ = (A_g^{1/2} u_\infty / \nu)\sqrt{c_f/2} \tag{3}$$

Its physical meaning is the transformation parameter of the area of the region through which the fluid flows in the cross-section of the riblet, and according to his drag reduction curves, it was found to have the best drag reduction at this dimensionless parameter of approximately 11 [75, 76], as shown in Figs. 2(c) and 2(d). More than 70% of the experiments performed by previous researchers [15] were experiments with V-shaped ribs, and in the experiments with air as the fluid, V-shaped ribs were the most common, followed by water and oil. Moreover, owing to the differences in experimental methods, some findings are different from the theory [70, 77], but most of them are in accordance with the laws mentioned above. Generally, under suitable parameter conditions, the riblet drag reduction has a value and significance for practical applications, with a drag reduction rate of approximately 8%–10%.

2.2.2 Drag reduction principles

There are two popularly accepted theories for the drag reduction principle of structures, namely, the protruding height theory and the secondary vortex theory. Previously, the riblet was considered ineffective for drag reduction because it increased the area in contact with the liquid [4]. However, with the progress of experiments and simulations, this notion gradually changed. Both the protruding height theory and the secondary vortex theory were first proposed by Bechert et al. [74, 78, 79]. He found and summarized the drag reduction principle of riblets through drag reduction experiments of various shapes of riblets in water and oil media, focusing on observations of the flow field and vortex, and through further analysis of the experimental results, the drag reduction principle of riblets is shown in Figs. 2(e) and 2(f).

The protruding height theory starts from the fact that the riblet sticks out of the wall and suggests that the presence of the riblet can influence the movement of the vortex between the two riblets. At the same time, the riblets that protrude into part of the flow field can raise the effective source flow by a certain distance. Thus, the location of the apparent source flow can be determined from the velocity. When the fluid flows in the groove, the limitation of the position of the apparent source flow affects the velocity distribution, which leads to thickening of the viscous substrate, a reduction in the velocity gradient, and ultimately a decrease in the resistance. The protruding height theory centers on the fact that the height of the protrusion affects the turbulence structure near the wall [5].

The secondary vortex theory centers on the fact that the vortex generated at the riblet tip location reduces the overall drag. Owing to the interaction of the riblet tip with the upper vortex, an opposite vortex is generated at the upper-middle position of the slot. This vortex causes the fluid in the lower and middle portions to be in less contact with the high-velocity fluid, resulting in a

reduced velocity gradient at the bottom as well as reduced drag. The top portion, on the other hand, has an increased velocity gradient and increased drag due to contact in the vortex, but the overall effect of the two parts depends on the shape and structure of the riblet. Within a reasonable parameter range, the bottom reduces drag more than the top increases it, which ultimately results in a reduction in drag. In addition to these two more popular theories, there are some other theoretical explanations. For example, Sasamori et al. [80] found that the presence of a riblet can inhibit the structure related to the two upper and low fluid exchanges on the near-wall surface, thus reducing the drag force. West et al. [81] argued that an increase in flow velocity reduced the boundary layer thickness near a wall, which exposed the ribs more to high-velocity fluid, thus weakening the drag reduction effect. Recently, Mawignon et al. [82] researched the effects of orientations and arrangements of three-dimensional rectangular cuboidal riblets on drag reduction. They reported that the region of high turbulent kinetic energy influenced the drag reduction rate. This can affect the wall shear stress of the riblets. They also introduce two theories. However, these methods are similar to those used in the research above. Compared with the imitation sharkskin structure, the drag reduction principle of the riblet structure is more explicit, but there is still room for further investigation.

2.3 Shrimp

2.3.1 Shape characteristics and research content

As a swift and ferocious predator in the ocean, the body structure of shrimp has evolved over a long period and has gradually adapted to the environment in the water with efficient locomotor performance. At the beginning of the 21st century, Stacey et al. [83] studied and analyzed the hunting process of shrimp and found that the structure of its abdomen can effectively reduce the vibration as well as the resistance of movement [83–85], and the body structure of the shrimp is shown in Fig. 3(a). It consists of the head, thorax, abdomen, tail, etc. The abdomen is the largest and consists of six segments, with the last segment connecting to the tail. The raised structure of the abdomen inspired Gu et al. [86] to study. He obtained the model by simplifying the structure of the abdomen and simulated it. The simulation model is shown in Fig. 3(b). By varying the shape parameters, speed and other factors, a maximum drag reduction of approximately 15% was obtained at a speed of 10 m/s. The simplified structure of the bellies of shrimp has practical value in real airfoils.

2.3.2 Drag reduction principles

According to the simulation results of Gu, the drag reduction principle can be summarized in two parts: on one hand, by increasing the thickness of the boundary layer, the velocity gradient is substantially reduced, which leads to a certain degree of reduction in both the shear stress and Reynolds stress at the wall surface, thus affecting the drag at the interface; on the other hand, this raised structure, which alters the structure of the flow field at the near-wall surface, creates a clockwise direction in the rear part of the raised vortex, as shown in Figs. 3(c) and 3(d). Converting the sliding of the fluid into rolling acts similarly to lubrication. Simultaneously, the vortex also affects the turbulent coherent structure, reducing the energy exchange between the high-velocity fluids and low-velocity fluids, thus reducing the drag. Owing to the lack of practical experiments, the drag reduction principle needs to be further explored.

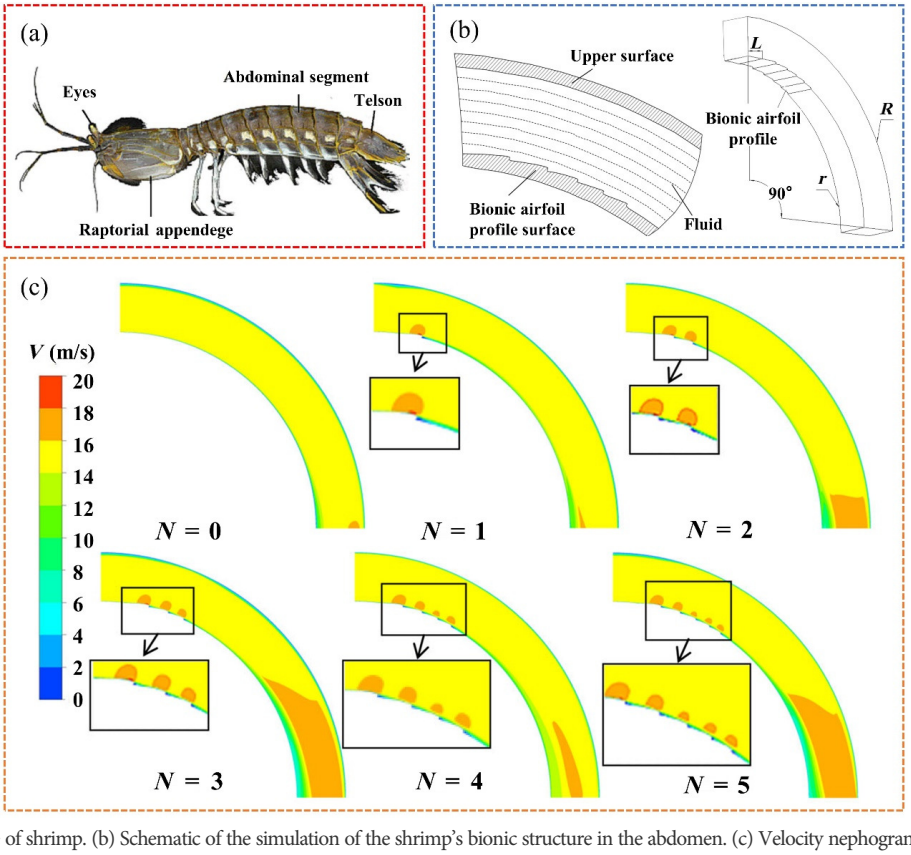

Fig. 3 (a) Body structure of shrimp. (b) Schematic of the simulation of the shrimp's bionic structure in the abdomen. (c) Velocity nephograms of different N (N is the number of structures). Reproduced with permission from Ref. [86], © Springer-Verlag GmbH Germany, part of Springer Nature 2020.

清華大学出版社 Tsinghua University Press | SciOpen

2.4 Loach

2.4.1 Shape characteristics and research content

This section discusses biological prototypes that use the scales of species other than sharks as the primary means of biomimicry, including categories such as loach and grass carp. In 2002, Sudo et al. [87] observed fish scales using a 3D measurement system (Mitaka NH-3), classified fish scales into four categories and measured the shape parameters of the scales, as shown in Fig. 4(a). It has been useful for subsequent studies on fish scales.

Afterward, Dou et al. [89] observed the microstructure of *Carassius auratus* scales by scanning electron microscopy and non-contact morphometry and found that the scales contained holes several micrometers in size. A similar surface was subsequently prepared by spraying and tested in a water hole, where a drag reduction of approximately 10% was obtained at a speed of 13 m/s. Then, Wu et al. [88] observed and analyzed the scales of grass carp, which were taken from the fins and back of the fish and processed accordingly, through scanning electron microscopy as well as field 3D microscopy. The observed results are shown in Figs. 4(b)–4(d).

The scales are divided into four parts: lateral, basal, apical, and scale focus. The basal part is the connection between the scales and the skin, and like the lateral part, it is usually covered by other scales. The top is exposed to the external flow field by staggering this model and analyzing it. Wu et al. [88] simplified the actual structure and built a crescent-shaped bionic structure, as shown in Fig. 4(e). This structure was tested under simulation and was found to yield the highest drag reduction rate of 3.014% at a speed of 0.66 m/s. In previous research, Wu et al. [90] used a laser engraving machine and a polishing machine to fabricate the surface of a real crescent structure, conducted drag reduction tests in a water tank built by themselves, and measured the contact

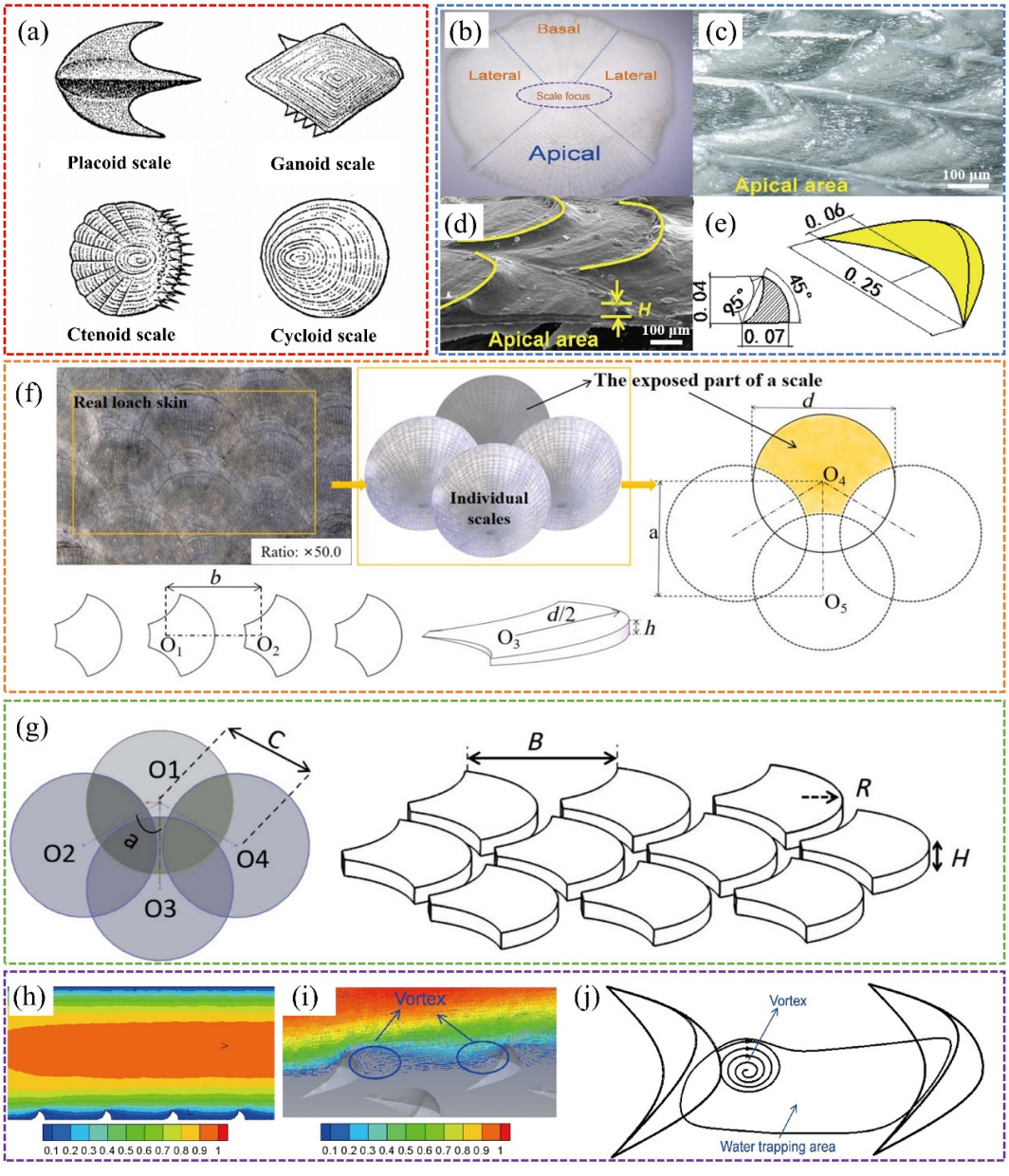

Fig. 4 (a) Four fish scale structures; (b) grass carp scale; (c) 3D view of scale; (d) SEM image of scale; (e) simplified view of crescent-shaped structure; (f, g) simplified unit structure of loach; (h, i) velocity cloud obtained from the simulation; (j) schematic diagram of drag reduction. Reproduced with permission from Ref. [88] for (b–e, h–j), © Science China Press and Springer-Verlag Berlin Heidelberg 2017.

angle. The data showed that the highest drag reduction of 2.805% could also be obtained at a speed of 0.66 m/s, confirming the previous simulation results. Moreover, the surface contact angle is approximately 11°, indicating the hydrophilicity of the material. Wu et al. [91] also investigated the surface scale structure of loaches by scanning electron microscopy and observed samples via 3D microscopy. The drag reduction characteristics of the imitation loach surface structure model were subsequently explored by simulation, and the highest drag reduction rate of approximately 2.2% was obtained. Then, they built two different types of models based on the previous observations: the model structures are shown in Figs. 4(f) and 4(g), and both models were simulated and experimented with: the first model was machined by a numerically controlled machine and experimented in a pipe with water as the medium, and at a velocity of 1.683 m/s, a drag reduction rate of approximately 23% was obtained; the second model was machined by the template replication method and tested in a water hole, and the test found that the highest drag reduction rate of approximately 17.25% could be obtained [92, 93]. Moreover, Monfared Mosghani et al. [94] arranged and simulated microstructures on a simulated hull by observing the pecten scale structure of fish and conducted experiments in a towing pool, and the highest drag reduction rate was approximately 20%. Wang et al. [95] investigated the morphology of *Sciaenops ocellatus*, extracted four mimetic scale microstructures, and prepared them via laser processing on aluminum alloy to prepare the surface with a structure, which was found to have hydrophobic properties and obtained a maximum drag reduction of 4.814% in laminar flow, while the drag reduction effect gradually disappeared under turbulent flow. Sun et al. [96] performed simulation experiments on fish scales and found that structured topological fish scale surfaces yielded a higher drag reduction rate of 5.35%. Recently, Yan et al. [97] explored the use of an imitation fish scale structure on the wing through simulation, explored the best combination by changing three parameters, namely overlap size, thickness, and coverage area, and studied and analyzed various parameters, such as speed and pressure, and finally obtained a drag reduction rate of 35.15%.

Most of the experiments and simulations were conducted with imitation fish scale structures. However, owing to factors such as observations and fish species, the bionic interfaces they obtained are not the same, which can also explain why the drag reduction rate and the conditions to reach the highest drag reduction rate are not consistent. Moreover, due to some errors in the observations, the ability to better mimic fish scales and make finer structures may further improve the drag reduction.

2.4.2 Drag reduction principles

For the drag reduction principle of the imitation fish scale structure, researchers have explored it in simulations and experiments, and due to the difference in the fish scale imitation structure, different imitations may have different drag reduction principles. For general scale-like microstructures in the order of a hundred micrometers, the researchers found that the values of turbulence data were smaller than those of smooth surfaces by outputting the turbulent kinetic energy and wall shear stress, indicating that scale-like structures can effectively reduce the degree of turbulent energy exchange and reduce the wall drag [95]. In addition, through the observation of the flow field, a vortex is observed on the leeward side of the structure, and this vortex plays a lubricating role, isolates the bottom low-speed fluid and the external high-speed fluid, and reduces the exchange of the flow between the upper and lower layers of the fluid, which results in drag reduction. The principle of drag reduction is shown in Figs. 4(h)–4(j). The changes in the components of drag with the use of microstructures were compared, and the results revealed that the shape drag increased, whereas the viscous drag decreased. With the right parameters, the falling value was greater than the rising value, resulting in a drag reduction effect. Moreover, the results of Rong et al. [22] show that the drag reduction effect can be further improved by combining other drag reduction principles, such as superhydrophobic surfaces, which also provides ideas for subsequent research on fish scale-like structures. In addition, for microstructures imitating the type of cavities on scales on the order of a few micrometres, Dou et al. [89] concluded that the air medium inside the structure contributed to the drag reduction rate.

2.5 Puffer

2.5.1 Shape characteristics and research content

The epidermis of the pufferfish possesses good flexibility [98] and is also distributed with cone-shaped protrusions [99], and in general, the surface drag reduction of the pufferfish is closely related to both. Here, the role of its protrusions in drag reduction is mainly discussed. Pufferfish reproduce through long-distance migration while overcoming the obstruction of water currents in the water, and at the same time, their migration, with essentially no food intake, implies that the energy consumption of pufferfish can be reduced during movement to meet the requirements for group survival. The morphology and surface characteristics of the spines of the pufferfish are shown in Fig. 5(a).

The spine protrusion of pufferfish consists of two main parts: the conical spinous process and the muti-claw spine base. Generally, the spine base is beneath the skin, and only the upper part of the spine protrudes into the external fluid. The length of the upper part is approximately 5/8 of the total length [100], and like other fishes, the surface of pufferfish is covered with a layer of mucus, which constitutes a complete epidermal structure. Zhou et al. accomplished curve recognition and reading of the spines through Photoshop and related software to construct a structural model of the protrusion and describe this structure with four parameters: height of the protrusion, radius at the bottom, curvature at the top, and curvature at the middle. Subsequently, a numerical simulation study was carried out, and at a water flow velocity of 5 m/s, the viscous resistance was reduced by 23.2%, while the total resistance was reduced by 12.94% [99]. Then, Fan et al. [101] investigated the influence of the protrusion arrangement and size on the drag reduction effect at two Reynolds numbers by analyzing turbulence data through water hole experiments and particle velocity measurement equipment and finally obtained a drag reduction rate ranging from 5% to 11%. Subsequently, the effects of several factors, such as the arrangement position and incoming flow angle, on the drag reduction effect were subsequently explored through simulation, and it was found that the greater the number of spines and the larger the spacing were, the better the drag reduction effect was, reaching 23.1% [102]. Zhou et al. [103] also analyzed data from water hole experiments through particle velocimetry to investigate the effects of protrusion height and arrangement on the drag reduction effect and found that when the protrusion height was lower and the arrangement was staggered, the highest drag reduction rate was 5.9%. Then, the effect of height and incoming flow angle was explored by simulation, and a drag reduction rate of approximately 20% was obtained [104]. In addition, Feng et al. [105] explored the drag reduction of flexible surfaces in combination with protrusions, prepared a total of five surfaces for

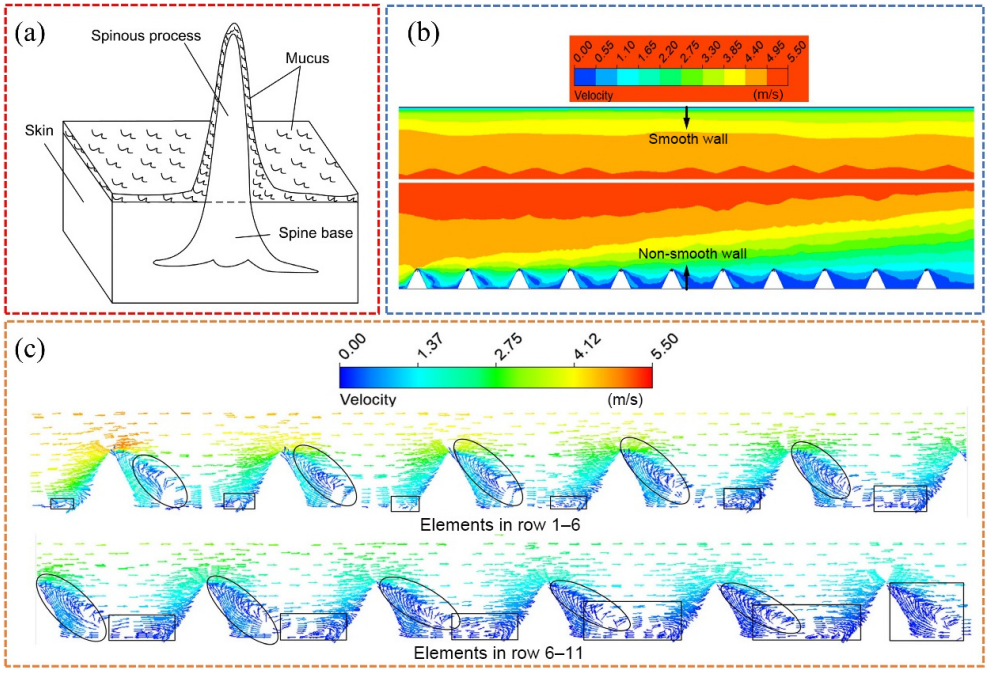

Fig. 5 (a) Spine model. (b) Velocity contours of simulation. (c) Velocity vectors of non-smooth plate. Reproduced with permission from Ref. [99], © Wiley Periodicals, Inc. 2020.

a controlled study, and obtained drag reduction rates ranging from 11.5% to 17.5% in turbulent flow. Tian et al. [106] performed a simulation study of the Reynolds number and height of the protrusion microstructure on a replica hull, analyzed the wake flow and other data, and finally obtained a drag reduction rate of 10%. The same research team recently explored the use of such raised microstructures by preparing elastic membranes with conical protrusions and performing water hole tests, obtaining a drag reduction rate of approximately 11%, which lays the foundation for practical applications [107].

Summarizing the above studies on drag reduction in imitation puffer fish surface structures, the data indicate that the drag reduction rate obtained from simulations is greater than that of actual experiments. Moreover, the elasticization of the microstructure helps improve the drag reduction rate of the microstructure; however, studies of the various influencing factors are not yet systematic enough, and there is no reasonable optimization of the overall parameters. In this regard, there is still room for further expansion. In addition, for the shape of the protrusion of the puffer fish, there is also variability, and the change rule of the suitable parameters can be analyzed under different experimental or simulation conditions to further elucidate the effect of drag reduction.

2.5.2 Drag reduction principles

By observing and analyzing simulation data such as wall shear stress and velocity field, Zhou et al. [103] found this raised structure had a reflux vortex upstream of it and an ascending vortex downstream of it, as shown in Figs. 5(b) and 5(c).

These two vortices, which effectively reduce the contact between the external high-velocity fluid and the bottom, play a certain lubrication role and reduce the turbulence intensity and dissipation rate, thus reducing the drag to a certain extent. Moreover, the analysis of the wall shear stress revealed that the Reynolds stress near the wall decreased, which directly represented a reduction in drag. Second, the presence of protrusions increases the shape drag and reduces the near-wall velocity gradient at the same time. Thus, again, it is necessary to reduce the value of viscous drag to greater than the increased value of drag to achieve drag reduction, which is similar to the Riblet principle. For the parameters of protrusion, such as height, the researcher also determined that with increasing height, although the viscous resistance decreased, the overall resistance increased, indicating that the shape resistance increased faster under the simulation parameters, which also confirms the drag reduction principle. While exploring the effect of incoming flow angle, it is found that a larger incoming flow angle leads to a lower drag reduction efficiency, and the drag reduction effect of the viscous term first increases, then decreases, and finally remains stable. This also explains the reason for the decrease in the overall drag reduction rate. Moreover, according to the above findings, when the imitation surface of a pufferfish is raised on an elastic surface, it can provide a better drag reduction effect, which illustrates the effectiveness of the combination of multiple methods.

2.6 Crocodile

2.6.1 Shape characteristics and research content

Crocodiles live in swamps, ponds, and other territories, and the skin structure of their abdomen as well as their flanks has attracted the attention of researchers because of their frequent movement in conditions of muddy water mixing [108]. As shown in Fig. 6(a), their abdomen is not smooth but consists of a variety of blocky hard skin, and the flanks are arranged differently. Yan et al. [108] modeled two kinds of shipboards by observing the arrangement of their epidermis, the torque type and the hexagonal shape, and conducted experiments in a constructed pool, which was specially formed to ensure the effectiveness and reliability of the experiments in an actual farmland situation with mud and water mixing. Subsequently, they conducted orthogonal experiments to investigate the effects of load, speed, and other factors; the highest drag reduction rate was approximately 6%, and they reported that the drag reduction effect of the rectangular structure was better

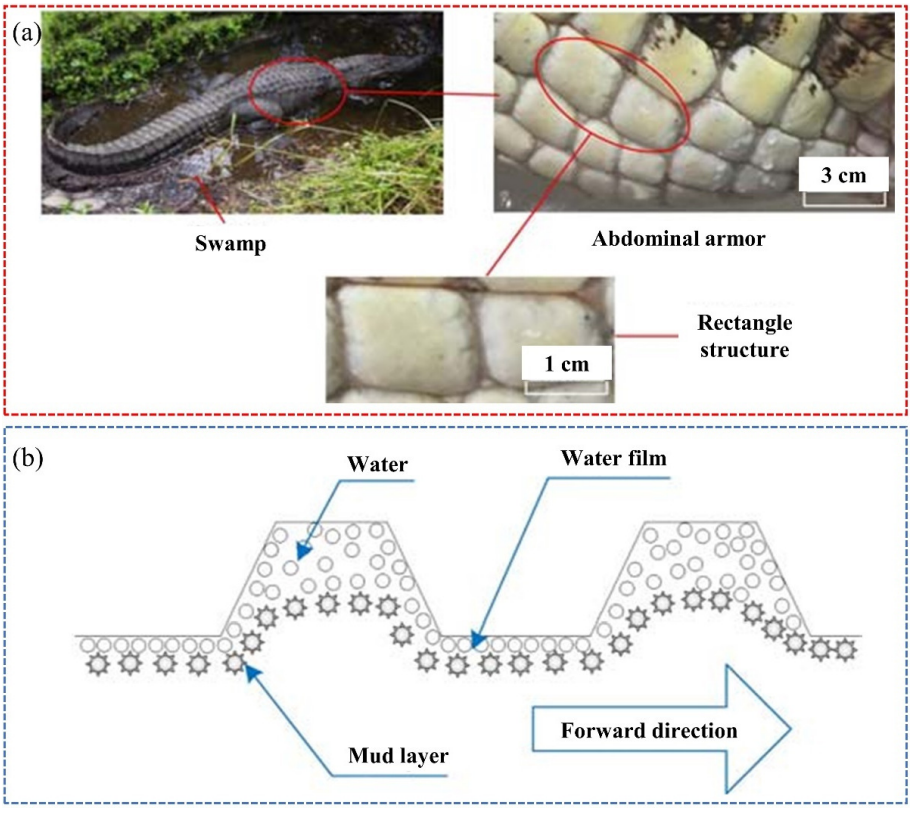

Fig. 6 (a) Step-by-step magnification of the abdomen of a crocodile. (b) Schematic diagram of water film theory. Reproduced with permission from Ref. [108], © International Journal of Agricultural and Biological Engineering 2020.

than that of the hexagonal structure, which is similar to the skin structure of the bottom of sea turtles, further verifying the rationality of the experiment.

2.6.2 Drag reduction principles

There is a similar explanatory theory for this principle of macrostructure drag reduction, namely, the water film theory [109], as shown in Fig. 6(b). Drawing on this theory, we explain the reason for the drag reduction effect obtained when the machine moves on the farmland. Due to gravity, the water seeps out of the mud and stagnates in the depressions of the block structure, and when there is relative motion between the block structure and the mud and water, the water present in the depressions therein will form a thicker film of water in the other areas than on the smooth surface. At the same time, because the pressure at the bottom is much lower, the water on both sides will also enter and thicken the water film, and the thickening of the water film prevents the direct viscous resistance between the bottom and the mud and acts as a lubricant, which directly reduces the actual resistance [108].

2.7 Dung beetle

2.7.1 Shape characteristics and research content

When living in dirt, the dung beetle can break up feces and compress and roll it into a ball shape. Moreover, the rapid movement of the dung beetle in the mud also proves that its epidermis has a better drag reduction effect. Therefore, the structure of its epidermis was carefully analyzed and studied by researchers [110], and the corresponding drag reduction effect was explored; its structure is shown in Fig. 7. By observing the structure of the crust of the dung beetle, Li et al. [111] found that there were many pits on it; then, they carried out clay friction experiments on the pits and obtained a drag reduction rate of approximately 5%, and their experimental samples were macroscopic structures on the millimeter scale. Tong et al. [110] further tested drag reduction on agricultural instruments with the presence of a raised structure on the test surface that mimicked the frontal plate of the clypeus of the dung beetles. Compared with those of the pufferfish, the protrusions were larger and flatter, and the pressure was reduced by approximately 10% by the addition of the microstructure. Afterwards, Kui et al. [112] added the pit structure to a diesel engine through simulation and found that the operating efficiency was higher than that of the original model. An et al. [113] used a pit and bump structure imitating a dung beetle on a rotator, and the effects of the size and arrangement of the surface structure were investigated by experiment and simulation. The test results showed that the rotator torque could be decreased by 11.7%. Sun et al. [114] investigated the use of dung beetle structures on equipment such as furrow openers, agricultural machinery, and centrifugal pumps [115–117] and reported that they reduced drag, resisted wear, or enhanced work efficiency, indicating that the bionic structures have the value and significance of practical use. Recently, Wang et al. [118] from Tsinghua University investigated the role of bumps on helmets and obtained a maximum of about 7% drag reduction, drag reduction of approximately 7%, while a delayed transition was found.

According to the literature, both pit and bump structures exist on the dung beetle; however, the meaning and significance of the distributions of these two structures have rarely been comprehensively analyzed, and their related parameters have not been studied in a more systematic statistical manner. However, the imitation structure can produce effects in several fields, and if the research can be further improved, it may be possible to further improve the efficiency of its use.

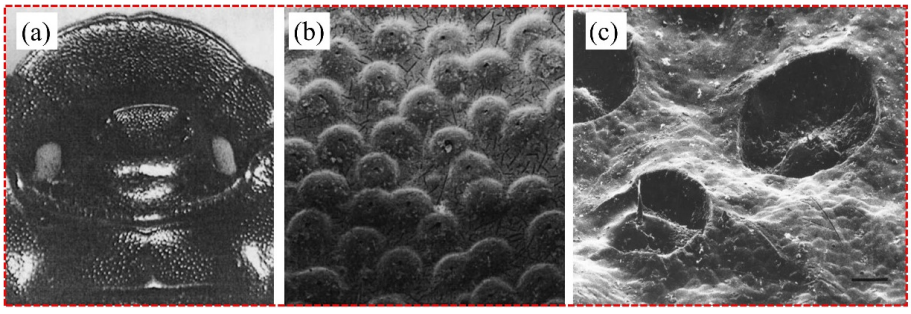

Fig. 7 (a) Stereoscopy image of the careruleus and pronotum. (b) Scanning electron microscopy image of the convex domes on the pronotum. (c) Pit structure of the head of a dung beetle. Reproduced with permission from Ref. [110] for (a, b), © Elsevier B.V. 2004.

2.7.2 Drag reduction principles

Since the pits and bumps of the imitation of the dung beetle are more macroscopic structures, they are slightly different from the drag reduction principle of the microstructure. Compared with that of the smooth surface, the pressure resistance of the pit surface is slightly greater, but the friction resistance is lower. An analysis of the surface flow field revealed that the pit structure can change the thickness of the boundary layer, as well as the related turbulence data, and reduce the velocity gradient to reduce the drag. At the same time, on certain equipment instruments, the dimple structure also serves to suppress the turbulence and reduce coherent structures. For the protruding structure of the imitation of the dung beetle, the drag reduction principle involves realizing drag reduction by generating a low velocity region between adjacent structures, which also increases the thickness of the boundary layer, reduces the energy exchange between the upper and lower flow fields, and carries out the lubrication between the flow fields [119].

2.8 Summary

Typical biological prototypes of surface structure bionic drag reduction methods and drag reduction principles are described in detail in this section. In general, the structure of biological surfaces is characterized by adaptation to the environment, and the surfaces with drag reduction effects or other functions can be prepared from their surface structure. The advantages of the bionic drag reduction method of surface structure are that it is simple, efficient, energy-saving, and has a wide range of applications, while the limitations are the restricted processing size, susceptibility to corrosion, and relatively weak laminar flow drag reduction effect. Taking the riblet structure as an example, it is simple in structure, does not require additional energy input, and can be used in various fields such as pipeline transportation and sports. From the point of view of the drag reduction principle, maintaining the effective structure size and increasing the forming area are the goals that can be further optimized.

3 Superhydrophobic surfaces

This section focuses on the research content and drag reduction mechanism of preparing drag-reducing functional surfaces modeled after natural superhydrophobic surfaces or structures, such as lotus flowers, water striders, and mosquito eyes.

3.1 Shape characteristics and research content

The concept of the contact angle of a liquid on a flat surface concerning that surface was first introduced by Young in 1805 [120]. Afterward, the contact angle was commonly used to measure the wettability of a plane to a liquid. When a liquid exists on a plane, it automatically reaches a state of minimum energy, so the contact angle can be measured and characterized. In general, for water droplets, hydrophilicity is distinguished on a flat surface by the magnitude of the contact angle, which is greater than 90° for hydrophobic surfaces and less than 90° for hydrophilic surfaces [121]. However, a plane can be called a superhydrophobic surface when the contact angle is greater than 150°and a superhydrophilic surface when it is less than 10° [122], as shown in Fig. 8(a).

Superhydrophobic surfaces have many good properties, including self-cleaning, corrosion resistance, drag reduction, and antifouling [8]. Therefore, superhydrophobic surfaces are highly practical. There are many types of superhydrophobic surfaces in nature, including lotus leaves, water spiders, mosquito eyes, dragonfly wings, rice leaves, and duck feathers. These types of superhydrophobic surfaces are found to have different kinds of microstructures and nanostructures after observation, as shown in Figs. 8(b)–8(e). The existence of these structures makes organisms more adaptable to the natural environment and allows researchers to find inspiration for their use in engineering. Understanding these natural superhydrophobic surfaces allows us to better prepare, detect, and utilize them to achieve many beneficial effects. The lotus leaf is one of the most typical superhydrophobic surfaces in nature. In 1997, Barthlott and Neinhuis [123] observed lotus leaf samples by scanning electron microscopy and reported many papillae-like protrusions on the surface, as well as the presence of a waxy layer, owing to which this structure is what endows the lotus leaf with superhydrophobicity. The water strider can move rapidly on the surface of the water without falling into the water. Gao and Jiang [124] also observed the leg structure of a water strider by scanning electron microscopy and reported a multilevel structure of the leg. It has a micrometer-scale bristle structure and a nanoscale groove structure, and measurements revealed that the contact angle of the water strider's foot was approximately 167°, which reached the theoretical level of superhydrophobicity. Moreover, this superhydrophobic structure allows the water strider to move freely on the water surface with the help of surface tension.

Fog systems can affect a variety of devices, such as eyeglasses and vehicles. However, in 2007, it was theorized that this problem could be solved by a superhydrophilic or superhydrophobic membrane, but the lotus leaf-like structure did not have an anti-fog effect. Gao et al. [127] found that mosquitoes had a composite structure with hundreds of ommatidia present at the micrometer level by observing their eye structure under a scanning electron microscope. As shown in Fig. 9(a), protrusions can be observed at the nanometer level, and since they are not easy to observe directly, Gao et al. [127] verified the effect of superhydrophobicity by preparing a bionic structure, as shown in Fig. 9(b), obtaining an average contact angle of approximately 155°.

Bixler and Bhushan [126] conducted an observational study on

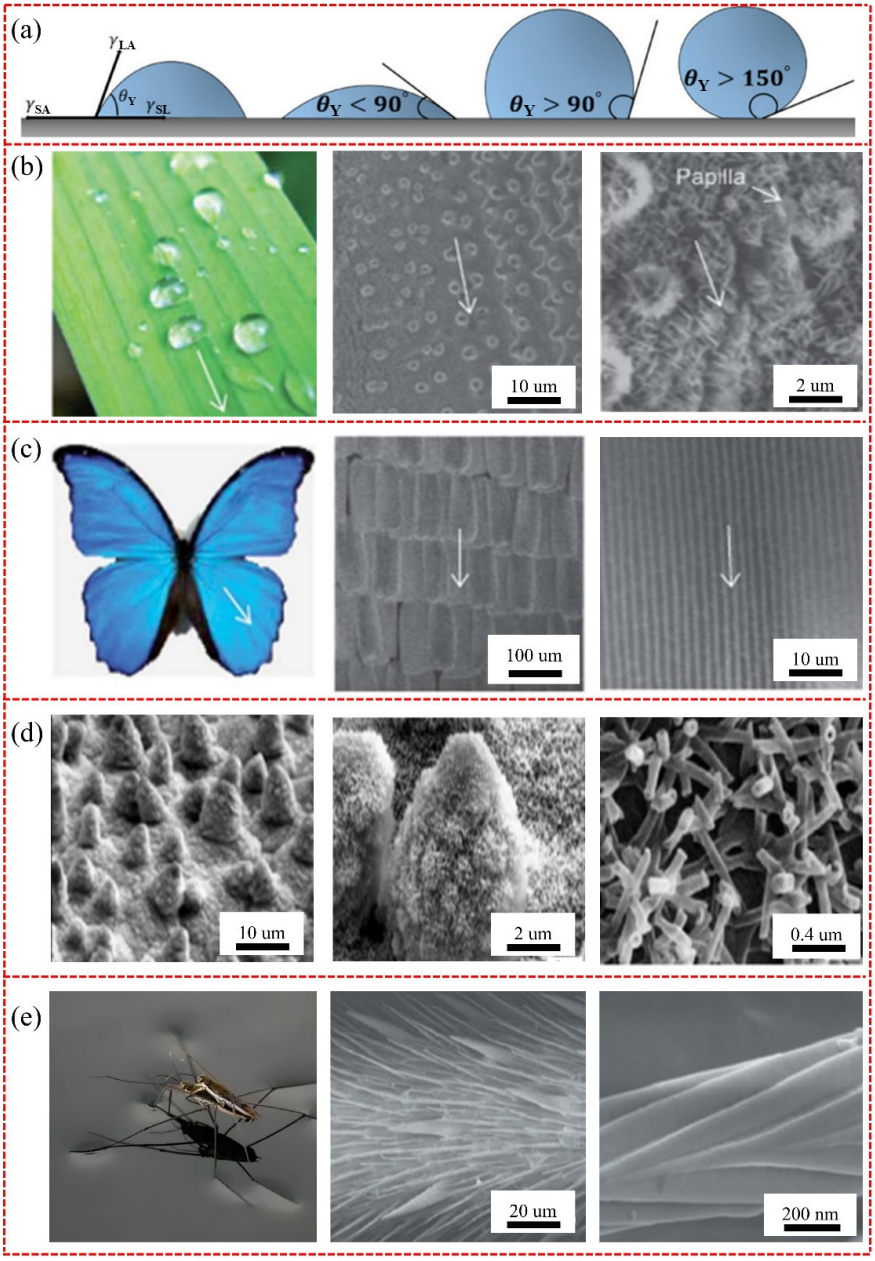

Fig. 8 (a) Schematic of contact angle. Microstructures and nanostructures of (b) rice leaves and (c) butterfly wings. (d) Morphology of lotus leaves at three magnifications. (e) Microstructures and nanostructures of water strider feet. Reproduced with permission from Ref. [125] for (a), © Elsevier B.V. 2023; from Ref. [126] for (b, c), © The Royal Society of Chemistry 2012; from Ref. [124] for (d, e), © Nature Publishing Group 2004.

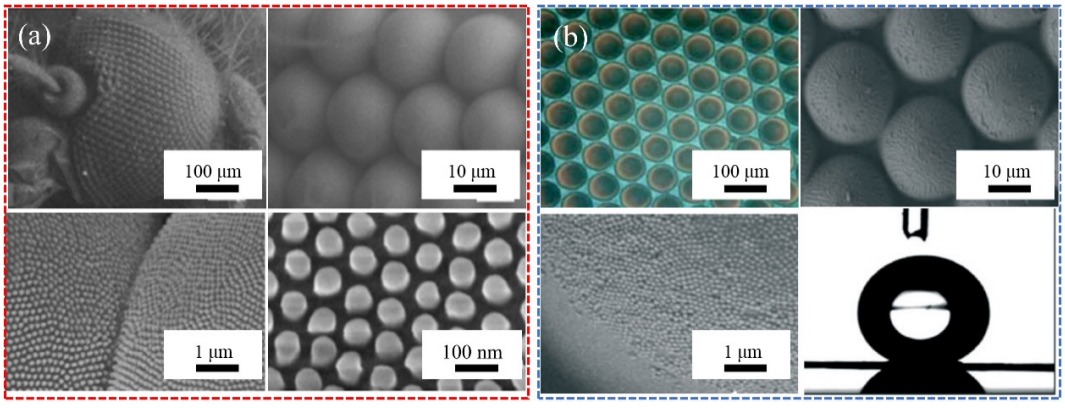

Fig. 9 (a) Step-by-step magnification of mosquito eyes. (b) Artificial structures that mimic mosquito eyes. Reproduced with permission from Ref. [127], © WILEY-VCH Verlag GmbH & Co. KGaA, Weinheim 2007.

the leaves of rice and the wings of butterflies. They found that they both possessed multilevel structures, with micrometer-scale sinusoidal fluctuations of grooves in the rice leaves and nanobumps in the grooves. Butterfly wings have micrometer-scale lamellar scales, and there are grooves on the scales. Rice is believed to grow in humid environments, and this superhydrophobic structure acts as a barrier to dirt and automatically cleans away dirt, thus reducing the impact on photosynthesis, while butterflies cannot clean their wings and therefore need special structures to ensure uninterrupted flight [128]. In addition, many organisms possess parts or surfaces with superhydrophobic properties [129, 130]. The data show that nearly 200 species of plant leaves have superhydrophobic properties. To summarize the characteristics of superhydrophobic structures, it can be found from the above studies that most superhydrophobic surfaces exist in multilevel structures, including at micrometer and nanometer scales. This multilevel structure has different shapes, with bristles, grooves, and scales at the micrometer level, grooves and bumps at the nanometer level, etc. The different kinds of structures also affect the realization of superhydrophobicity and the contact angle, which in turn affects the functionality and reflects the adaptation of organisms to the natural world over a long period of evolution.

With so many structural features, superhydrophobic surfaces also have drag reduction properties. In 2002, Kim and Kim [131] prepared superhydrophobic surfaces and conducted experiments on both flat plates and pipes, and found that the drag reduction effect could be realized by greatly reducing the resistance between the fluid and the wall. As a result, subsequent researchers investigated the drag reduction effect of superhydrophobic surfaces. Henoch et al. [132] subsequently prepared a superhydrophobic surface on aluminum using photolithography plus ion reactive etching technique and tested it in a water hole, obtaining a drag reduction of approximately 50%. Daniello et al. [133] measured the drag reduction properties of superhydrophobic surfaces under turbulent conditions using particle velocimetry technique as well as differential pressure measurement equipment and obtained up to approximately 50% drag reduction. At the same time, they found that a critical Reynolds number existed such that the drag reduction effect started to appear when the thickness of the viscous substrate in the boundary layer reached the size of the superhydrophobic surface. Du et al. [134] reported that the gas layer contained in a superhydrophobic surface could be restored by air injection through a combined method of air injection plus a superhydrophobic surface, maintaining the gas in the surface structure, and up to approximately 20% drag reduction was obtained in a water pipeline. In the same year, Taghvaei et al. [135] prepared a superhydrophobic surface via spraying of micron-sized particles plus nano-sized particles. It was tested in a towing pool, and a drag reduction of 7%–77% was obtained at Reynolds numbers from 47,000 to 235,000, as well as good stability in water, which is of good practical value. Monfared et al. [136] machined grooves by wire-cutting technique, prepared multistage structures through a series of chemical reactions, tested the pressure drop in a closed flume, and found that both untreated riblet and superhydrophobic-treated riblet had a drag-reducing effect but that the treatment dramatically increased the drag reduction rate to 56.9%. Similar to previous work, Hu and Yao [137] conducted resistance test experiments on superhydrophobic riblet composite surfaces, superhydrophobic surfaces, and smooth surfaces in a water hole and found that the composite structure could maintain approximately 20.2% drag reduction at relatively high Reynolds numbers, which was better than the effect of superhydrophobic surfaces alone.

In addition to the experiments on drag reduction mentioned above, there is also work on superhydrophobic surfaces through simulation. In 2004, Min and Kim [138] investigated superhydrophobic surfaces by direct numerical simulation and found longitudinal slip drag reduction and transverse slip drag increase on hydrophobic surfaces under slip boundary conditions. Two years later, Fukagata et al. [139] used theoretical calculations to predict the effect of drag reduction on superhydrophobic surfaces, and the results matched those of direct numerical simulations. Nouri et al. [140] obtained the drag reduction rate of a pipe under turbulent flow conditions through theoretical calculations and predicted the drag reduction effect by adding the slip boundary condition to large eddy simulation equations; the predicted results can be matched with those obtained by direct numerical simulation (DNS) methods. Nouri et al. [141] investigated the effects of factors such as shear rate on the drag reduction effect on superhydrophobic surfaces using large eddy simulations and found that higher shear rates resulted in greater drag reduction. Park et al. [142] used direct numerical simulations to investigate the fluid conditions in superhydrophobic pipelines and reported that the effective slip rate was higher in laminar flow than in laminar flow. Under laminar flow, the effective slip length was related to the shape of the slot but not to the Reynolds number. In turbulent flow, the effective slip length is a function of Reynolds number, and it was also found that the drag reduction on superhydrophobic surfaces was better in turbulent flow than in laminar flow. Cheng et al. [143] conducted a numerical simulation study of micro-pipes with superhydrophobic surfaces inside and investigated the drag reduction properties of micro-structures such as columns, holes, transverse grooves, and longitudinal grooves and found that groove structures had better drag reduction properties. Jung et al. [144] investigated pipe flow under turbulent conditions by direct numerical simulation, simplified the liquid–air interface as a flat surface, neglected the effect of surface tension, and found that the thicker the air layer was, the greater the slip length, slip velocity, and drag reduction rate were. The drag reduction rate fluctuates roughly within the 10%–90% interval. Li et al. [145] used the volume of a fluid model to study the drag reduction effect of slip on superhydrophobic walls under laminar flow conditions and explored the influence of factors such as shape on the drag reduction effect. The drag reduction effect increases when the cavity ratio rises and the pipe height decreases, and among the four cavity shapes, namely, triangle, wedge, rectangle, and trapezoid, the wedge shape is found to have the best drag reduction effect. Moreover, the parabolic shaped gas–liquid surface was found to be more in line with the real situation than the plane model simplified earlier [145]. Afterwards, Im and Lee [146] used a direct numerical simulation approach to simulate round and rectangular tubes with fully developed turbulence, using no-slip plus free-shear boundary conditions, taking into account the effects of the cycle length and superhydrophobic area share factors. The drag reduction rate increases when these two factors increase, and the simulations show that the circular pipe is more effective than the rectangular pipe. In addition, mathematical analysis has shown that the presence of strong secondary flow due to the increased spreading slip of the pipe flow has a greater attenuating effect on vortex transport than the channel flow, which leads to a higher drag reduction rate. Mollicone et al. [147] used a direct numerical simulation method and found that superhydrophobic surfaces can reduce the flow separation points of nonfluidic forms, as well as the size of separation bubbles, with a size reduction of approximately 35%. Nguyen et al. [148] used a direct numerical modeling approach to study solid surface occupancies of 1/16, 1/11, and 1/4, respectively,

of different arrangements of the species with drag reduction effects, including uniform, staggered, and random, with smooth surfaces on the upper surface and superhydrophobic surfaces on the lower surface of the watershed model. The highest drag reduction of 42% was obtained at 1/16 solid occupancy with a uniform arrangement. An analysis of the turbulence data revealed that the superhydrophobic surface changed the generation, transfer, and dissipation of turbulence. Recently, Safari et al. [149] found that the superhydrophobic surfaces altered the characteristics of the peak Reynolds stresses, their locations, etc., implying that the wall shear stress decreases and thus the drag decreases. A comparison of three models, Reynolds-averaged Navier–Stokes (RANS), detached eddy simulation (DES), and large eddy simulation (LES), reveals that LES has the best matching characteristics with the experimental results, and the simulation study of superhydrophobic surfaces revealed up to 48.9% drag reduction.

Other scholars have investigated superhydrophobic drag reduction in laminar and turbulent flows [150, 151] and have summarized the previous work. As shown in Fig. 10, the structure, size, and gas ratio of superhydrophobic surfaces affect the drag reduction effect. There is a large variation in the drag reduction of different superhydrophobic structures, ranging from 5% to 90%, as well as a link with slip length. The equipment used for the experimental study includes water holes, drag pools, pipes, viscometers, rheometers, and so on. The gas layer on superhydrophobic surfaces tends to fail at high speeds or high pressures, which affects the surface drag reduction. Moreover, different experiments have prepared superhydrophobic surfaces via different processes, such as photolithography, spraying, and replication, producing various morphologies that are random and homogeneous. Overall, superhydrophobic surfaces can achieve a higher drag reduction rate than microstructures and have various functions, such as self-cleaning and antifouling. For the simulation results of superhydrophobic surfaces, the most commonly used computational model is direct numerical simulation, followed by other types of models, such as LES. In addition, for the simulation of superhydrophobic surfaces, the most commonly used methods are no-slip walls and boundary setting of free shear wall. Moreover, simulation studies of superhydrophobic surfaces can match the drag reduction effect with the experimental values in most cases, with few deviations due to the effect of gas layer instability or simplifications of the simulations performed. Factors such as slip length, Reynolds number, and solid contact area percentage appear most frequently in studies of superhydrophobic drag reduction cases. Through a combination of simulations and experiments, researchers have investigated the mechanism of drag reduction for superhydrophobic structures.

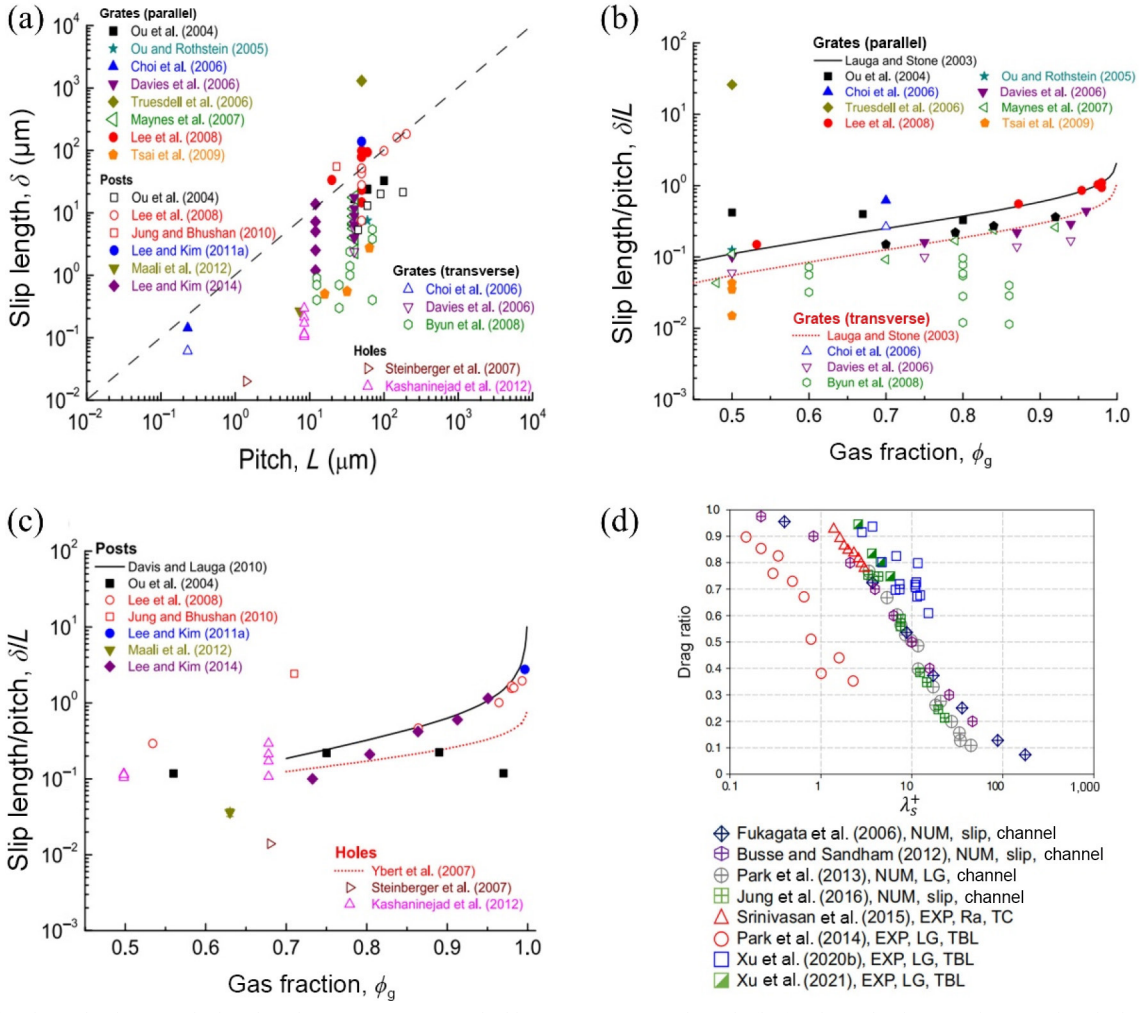

Fig. 10 (a) Relationship between slip length and structure spacing. Dashed lines represent general trends. (b, c) Relationship between dimensionless slip length and air ratio. Lines represent theoretical predictions [151]. (d) Resistance ratio varies with dimensionless slip length: LG for grooves, Ra for random roughness, NUM for numerical simulation results, and EXP for experimental results [150]. Reproduced with permission from Ref. [150], © The Author(s) 2021; Ref. [151], © The Author(s) 2016.

3.2 Drag reduction principles

A more common explanation for the drag reduction mechanism on superhydrophobic surfaces is the effective slip length theory [13, 121, 152], as shown in Fig. 11(a).

In general, there is no slip in the contact between the solid and liquid. In contrast, for superhydrophobic surfaces, the presence of air as the water layer flows over it can cause the liquid to slip on the surface [153]. The slip effect can be characterized using slip length. The slip length is the distance that is projected into the wall to obtain a vanishing velocity under no-slip boundary conditions. When the slip length is within a suitable range that satisfies the need for fluid characteristic length, then a certain drag reduction effect occurs. In addition, the drag reduction effect can also be explained by converting the solid–liquid interfacial contact into solid–gas interfacial contact, which is one of the main reasons for the very high drag reduction effect of the superhydrophobic wall. Under laminar flow conditions, the geometry of the superhydrophobic surface structure and the slip length mentioned above are the main factors affecting the drag reduction rate. Under turbulent flow conditions, various factors, such as Reynolds number and slip length, influence the drag reduction effect. Moreover, according to the simulation results, the drag reduction rate of superhydrophobic surfaces is generally greater in turbulent flow than in laminar flow. Superhydrophobic surfaces on near-wall surfaces affect turbulence generation, development, and dissipation, such as inhibiting turbulent coherent structures. Moreover, the presence of superhydrophobic structures causes a significant upward shift in the logarithmic region of the mean velocity at the near-wall surface, while attenuating the flow pulsation, which is partly responsible for the drag reduction. In addition, the study of the flow field reveals that the superhydrophobic surface recognizes more small-scale structures and fewer large-scale structures, implying that the energy transfer in the direction perpendicular to the wall is suppressed, reducing the wall friction resistance. To achieve the drag reduction effect of superhydrophobicity, the surface structure should generate a sufficiently large slip, the scale should try to meet the requirements of viscous substrate, and the shape characteristics, as shown in Fig. 11(b), should preferably have a multistage structure to ensure the stability of the gas.

3.3 Summary

Superhydrophobic bionic drag reduction methods have many excellent properties and can achieve high drag reduction rates under specific circumstances. In terms of structural characteristics and the drag reduction principle, its advantages include self-cleaning, anti-corrosion, and laminar turbulence effectiveness, etc., and its structure is generally a nano–micron composite structure. Therefore, its limitations are poor durability, relatively high processing cost, and limited adaptability to the actual environment, and its preserved gas layer easily escapes with increasing pressure, resulting in weakening of the drag reduction effect or even increasing drag, which is also a major problem of the superhydrophobic structure drag reduction method. For follow-up research, the biological prototypes of the study can be expanded to obtain more effective superhydrophobic structures [129, 130], which can further improve the stability of superhydrophobic structures under high flow rates or high pressure and realize better practical applications.

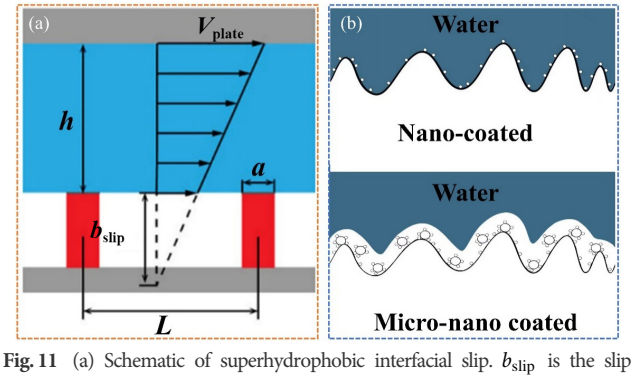

Fig. 11 (a) Schematic of superhydrophobic interfacial slip. b_{slip} is the slip length; h is the thickness of the laminar flow; V_{plate} is the velocity of the flat plate; a is the width of the grooves; L is the spacing between the two neighboring grooves [143]. (b) Multi-stage structure effectively protects the gas layer. Reproduced with permission from Ref. [152], © The Author(s) 2022.

4 Compliant wall

This chapter focuses on a drag reduction method that uses dolphins as the main bionic object, namely, the compliant wall drag reduction method. The method has a long history of research, and the following section describes the characteristics of the surface and the principles of drag reduction.

4.1 Shape characteristics and research content

The origins of the compliant wall drag reduction method, in which the dolphin is the main bionic object, can be traced back to Gray's paradox in 1936 [154], in which Gray calculated that, to satisfy the speed requirements of a dolphin's movement in the water, the force generated by the dolphin's muscles was seven times greater than that generated by the muscles of a normal human paddler [155]. Although this paradox has been explained by many researchers with further studies [156, 157], including speed and muscle differences, Gray's conjecture that the dolphin's surface functions as a delayed transition mechanism has sparked exploration and research by subsequent researchers. Unlike the shark surface, the dolphin surface is very smooth, with a roughness of approximately 2.5 μm [158]. The normal movement speed of dolphins is approximately 1–4 m/s, and the burst speed can reach 10 m/s. The speeds of different species of dolphin may differ slightly, but dolphin surfaces should have a drag reduction principle different from that of sharks to survive in the water, experience a long period of natural selection and be able to be maintained quickly. The surface structure of a dolphin is shown in Fig. 12(a).

From the surface to the interior, the structure consists of epidermis, dermis, papillae, dermal ridges, and sebaceous layer. This epidermal structure endows the dolphin surface with excellent elasticity [159]. Most of the layers are 0.5–3 mm thick and vary between different species. Researchers have shown that papillae on a dolphin's surface can sense the pressure of water flowing over them, allowing the dolphin's body fluids to enter or leave bumps based on the sensed information, which allows the volume of the papillae to change. As a result, the dolphin's skin expands or contracts [162], resulting in folds or vibrations. Such a property affects the flow of water over the epidermis, changing the structure of the flow field. This change is generally believed to benefit dolphin movement in water by reducing resistance to flow. Inspired by the structure of the dolphin epidermis, researchers have begun to investigate the drag-reducing effects of compliant walls and their practical applications.

The earliest experimental research on compliant walls was conducted around the 1960s by Kramer [163–165], who achieved up to approximately 50% drag reduction by mimicking the epidermis of a dolphin to create a flexible coating. Researchers

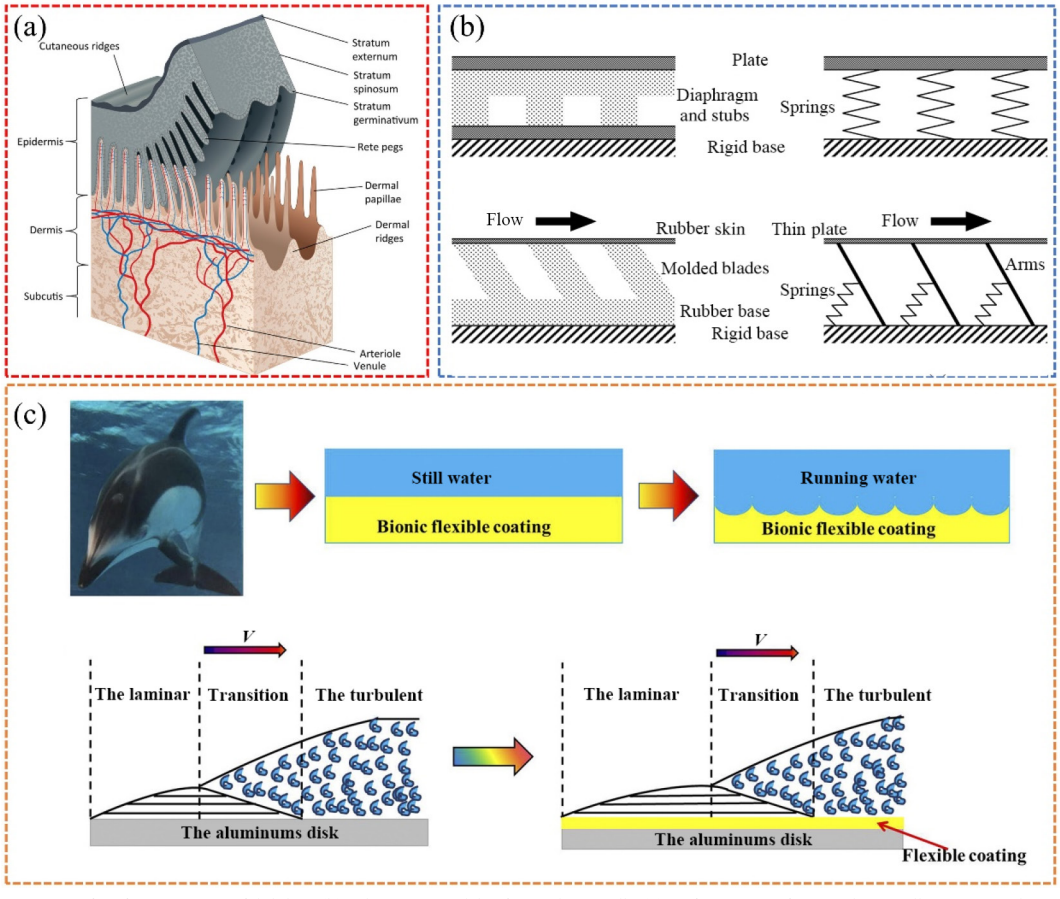

Fig. 12 (a) Composition of surface structure of dolphin. (b) Schematic models of compliant walls. (c) Deformation of a compliant wall in water and model of the delayed transition of a compliant wall. Reproduced with permission from Ref. [159] for (a), © Elsevier Inc. 2016; from Ref. [160] for (b), © Taylor & Francis 2008; from Ref. [161] for (c), © The Author(s) 2020.

subsequently began a series of experiments that showed different results, with some experiments finding an increase in drag while testing the compliant wall [166]. In 1985, Carpenter et al. [167] found through theoretical calculations that the compliant wall could indeed delay the transition of laminar flow while explaining the failure of the previous experimental results. Thus, theoretical and simulation studies began to be further developed after this, and several experiments for theoretical validation were also conducted. Carpenter further optimized the drag reduction effect of compliant walls and achieved theoretical predictions of traveling-wave flutter and divergence instability. Choi et al. [168] conducted drag reduction tests in water caves with compliant wall surfaces prepared from silicone rubber materials. A drag reduction of up to 7% was obtained in the velocity interval of 2–6 m/s, and the compliant wall effectively reduced wall friction and velocity fluctuations, shifted the logarithmic region within the boundary layer upward, thickened the viscous substrate, and ultimately affected the turbulence structure and strength. Afterward, Gad-el-Hak [166] provided a theoretical summary of previous studies, systematically stating the principles of dolphin drag reduction as well as the traveling wave theory. Nagamine et al. [169] conducted experimental and simulation studies to model the structure of compliant wall surfaces and found that compliant walls can reduce the number of vortices at the wall and influence the turbulent structure of the wall, thereby reducing shear stresses and ultimately drag. A significant portion of the compliant wall material used to conduct the experiments was a composite structure of silicone rubber. However, the time that it has effects is not long. Simulation tests of compliant walls have also been carried out by researchers. Fukaga et al. [160] investigated the flow and drag reduction characteristics of anisotropic flexible surfaces inside a pipe through direct numerical simulations, optimizing the parameters through an evolutionary algorithm, and obtaining up to 8% drag reduction. Several simplified models of compliant walls are given in Fig. 12(b).

In the same year, direct numerical simulations performed by Matsumura et al. [170] found that the near-wall turbulence intensity and shear stresses were reduced for compliant walls. Subsequently, Lee et al. [171], Boiko et al. [172], and others experimented with compliant walls in experimental facilities such as water and wind tunnels and obtained a drag reduction of approximately 5%. With the further development of this research, practical applications have also begun to appear. Shang et al. [173] applied the compliant wall structure to centrifugal pumps to achieve an approximately 5% efficiency improvement, and the study showed that the bionic surface can effectively reduce the differential pressure resistance, density of vortices, and velocity of the near-wall surface, thus reducing the energy dissipation. Schrader [174] conducted a simulation and experimental investigation on the drag reduction effect of compliant walls. The simulation model was RANS, while the experiment was conducted in a water cave, and the prepared compliant wall materials were silicone polymers and polyethylene films, which theoretically yielded a maximum drag reduction of approximately 3%. Chen et al. [175] explored the drag reduction effect of approximate periodic elastic support row surfaces. The highest

drag reduction rate of 72.16% was obtained, and this surface facilitates the maintenance of stability in the boundary layer and delays the onset of transition. This study expands the structural composition of compliant walls.

Overall, the early experimental studies before 1985 had widely varying results and belonged to the experimental exploration phase. Subsequently, between 1985 and 2000, theoretical studies on traveling wave damping in compliant walls began to develop, exploring and proving mechanisms. Furthermore, theoretical and simulation studies were further developed to guide the experiments, and practical applications began to appear, with more types of compliant wall materials being put into use, further expanding the research content, including the effects of aging, mechanical properties and other factors on the damping effect. At the same time, the optimization of the parameters of the compliant wall is also an important research topic.

4.2 Drag reduction principles

The drag reduction principle of compliant walls can be generally categorized into two aspects [161, 176], the first being more basic, delayed transition, as shown in Fig. 12(c). Theoretical calculations reveal that the compliant wall can indeed extend the interval of laminar flow, and from fluid dynamics, the resistance of turbulence is several times greater than the resistance of laminar flow; thus, delayed transition means that more area is in the state of laminar flow with lower resistance, which results in a greater drag reduction effect. Furthermore, the delay in transition comes from the interaction between the fluid and the compliant wall. On one hand, the compliant wall suppresses the pressure fluctuation of the fluid and absorbs part of the turbulent kinetic energy. On the other hand, the surface deformation of the compliant wall increases the thickness of the boundary layer. In addition, the fluctuation generated by the absorbing energy of compliant wall is not as high as it is when the fluctuation breaks through the boundary layer but will lead to an increase in the turbulence intensity and resistance, which is why some of the experiments have produced increasing resistance. Moreover, the compliant wall generally has a low surface roughness, so the shape resistance is low, and after the realization of the delayed transition, a high rate of drag reduction can be achieved. The second is boundary layer perturbation theory. Delayed transition cannot explain the drag reduction effect of compliant walls in the case of complete turbulence. Therefore, researchers believe that the compliant wall can interact with the boundary layer to reduce the pressure by absorbing energy, making the turbulent layer far away from the wall, which is explained by traveling wave theory. The influence of the compliant wall has both a local effect and a wide range of effects, and a local increase in the Reynolds stress is not conducive to stability. However, the compliant wall reduces the energy of Reynolds stress generation at a wide range of scales and stabilizes the Tollmien–Schlichting fluctuations, thus achieving a reduction in drag. In addition, the compliant wall has been shown to have an inhibitory effect on the vortices near the wall, which reduces the density of the vortices near the wall, thus reducing the turbulence intensity and the wall shear stress. Overall, delayed transition and interaction with the boundary layer are the main reasons for drag reduction in compliant walls, but more mechanisms need to be further explored.

4.3 Summary

The compliant wall drag reduction method with dolphins as the main biological prototype has been studied a lot experimentally, theoretically, and simulatively [169]. In general, the compliant wall has the advantages of good self-adaptation, energy saving, and a significant drag reduction effect. The compliant wall can generate corresponding fluctuations according to the flow field to reduce drag, and the drag reduction rate is relatively high. However, the design and manufacture of compliant walls are more complex [160], with a variety of models, and the cost of maintenance is also higher. Future studies can start from the principle of the compliant wall through better structural design [175] and better material selection to further improve the drag reduction rate and reduce the cost of use.

5 Polymer additives

In this chapter, the research on mucus is described in terms of fish mucus, concluding that the polymers contained therein are an important factor in the source of the drag reduction effect based on the composition of fish mucus, and then, the research on polymers and the mechanism of drag reduction is described.

5.1 Characteristics and research content

For both sharks in the ocean and grass carp in freshwater, a thin layer of mucus exists on the surface of most fish, resulting in a slippery sensation when they are touched [177]. In the human body, such as bronchial tubes, mucus is also secreted and has effects such as removing foreign bodies [178, 179], but its function is not drag reduction. Therefore, this part of the paper focuses on exploring the study of polymer additives using fish mucus as a biomimetic material. Fish mucus has various functions, such as preventing pollution and reducing drag, and plays an important role in the survival of fish. According to the summary of Hoyt [180], as early as 1929, Magan et al. conducted movement tests on fish and found that their gliding resistance was greater than that of the streamlined model. As a result, many subsequent researchers began to conduct resistance tests on fish and have investigated the role that fish mucus played in drag reduction. Afterward, Hoyt [180] mixed the surface mucus of marine fish with seawater and compared it with that of pure seawater and found that it could reduce the flow resistance by approximately 14%. Rosen and Cornford [181] found that fish mucus failed rapidly when it was detached from the body, losing approximately 25% of its original drag reduction in 3 h. At that time, researchers were not able to accurately determine the composition of fish slime. In 1981, Daniel [182] found that the difference in viscosity between fish slime and water was only one centipoise by performing density and viscosity measurements of fish slime. In addition, Parrish and Kroen [183] examined the mucus release rate of Menidia and observed whether there was a difference in the oscillation frequency of the fish by adding polymers to the water and found that polymers in solution did not affect the drag reduction effect of the fish. Subsequently, with the advancement of science and technology, Fudge et al. [184] studied the mechanical properties and composition of hagfish mucus and found that 99.996% of the components of the mucus of this fish were water, 0.0015% mucin, and 0.002% thread polymers; they also carried out the extraction of the mucus and observed, as shown in Figs. 13(a) and 13(b). Moreover, weighing of the fish revealed that mucus constituted 3%–4% of the total mass of the fish. However, for the mucus analysis of loaches, the weight of components other than water is only approximately 0.5% of the total mass of the mucus, and these components include proteins, fats, inorganic salts, and sugars. Moreover, the pH value of the mucus is near 7, which is neutral [177].

Later, Yanuar et al. [186, 187], Wood [188], and other researchers successively coated mucus on the hull model, tested

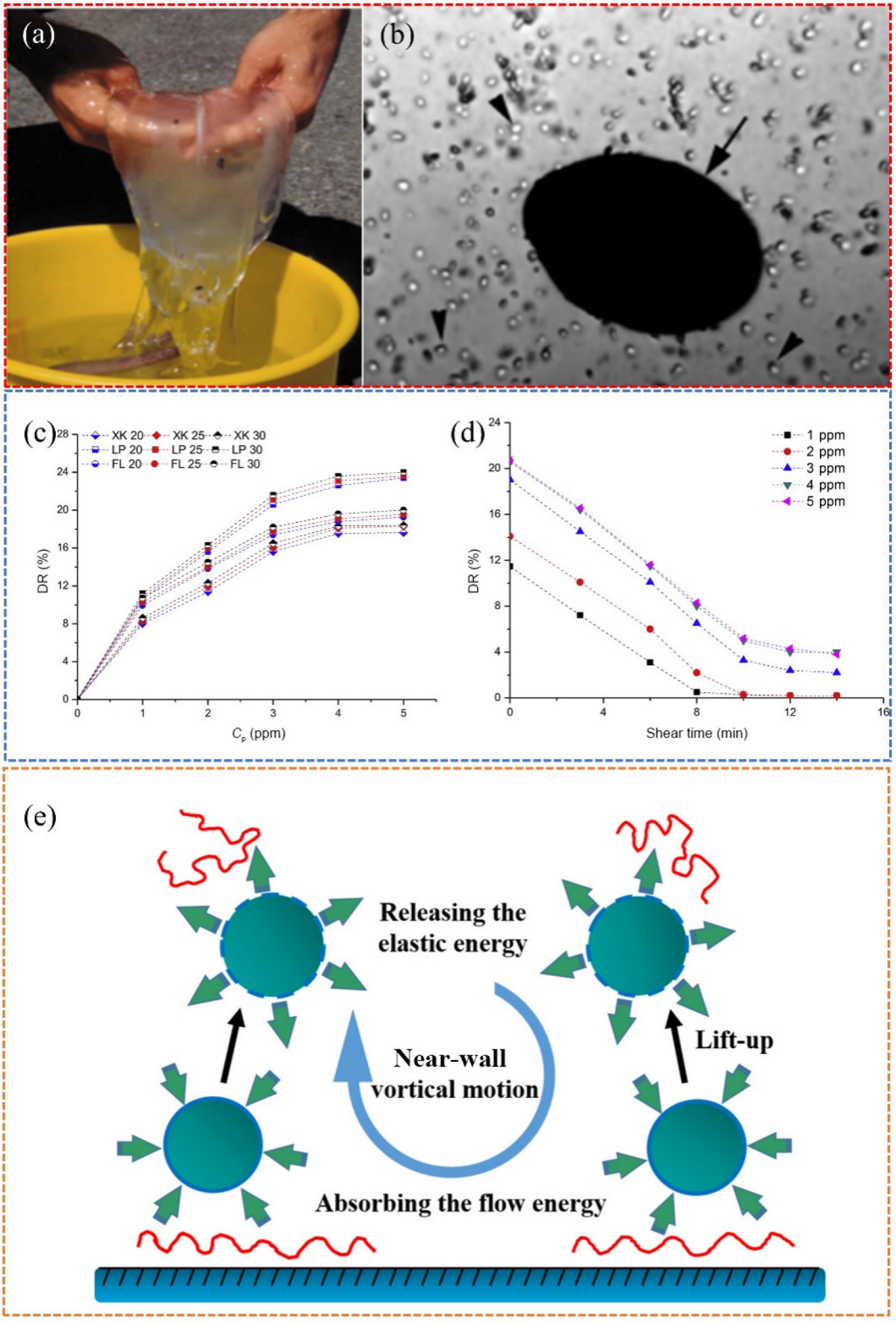

Fig. 13 (a) Extracted fish mucus. (b) Microscopic magnified image of the fish mucus. (c) Temperature dependence of drag reduction associated with different drag reducers and concentrations of a diesel oil system. (d) Shear time dependence of drag reduction associated with different drag reducers at 1.5 m/s. (e) Theoretical schematic of polymer drag reduction elastic theory. Reproduced with permission from Ref. [184] for (a, b), © The Company of Biologists Ltd. 2005; from Ref. [185] for (c, d), © Elsevier B.V. 2019.

the drag reduction, and obtained an approximately 10% drag reduction rate. Moreover, simulations of fish slime have also been carried out, such as the work of Tian [189] and Zhang et al. [190], who simulated the slime damping test via constitutive equations or multiphase flow and obtained a damping reduction rate of approximately 20%. Research on fish mucus has led to consideration on the intrinsic mechanism of drag reduction in terms of composition; since most of the components are water and the remaining components account for a very small percentage, the components of this source of drag reduction

should function at a low concentration. As the study progressed, it was eventually concluded that the polymer in the mucus was the direct source of the drag reduction effect, and it was found that the polymer could produce a significant drag reduction effect at a level of only 1 ppm, which was able to match the level of the fish component [185]. This also allows researchers to study the damping effect of polymers and the underlying theory from the perspective of fish-like mucus, thus explaining the mechanism of the damping effect of fish mucus.

The polymer drag reduction can be traced back to 1948, when Tom published the results of his experiments on polymer degradation, in which he found that polymers had a significant drag reduction effect at high Reynolds numbers. Therefore, the polymer drag reduction effect is also called "Tom's effect" [191]. An increasing number of researchers have subsequently begun to study polymer drag reduction. In 1967, Virk et al. [192] summarized previous experiments, systematically investigated the relationship between polymer drag reduction and concentration, and discovered the phenomena of the onset and maximum drag reduction points of polymer drag reduction effect. The former implies that polymers need to reach certain conditions, such as the concentration or number of macromolecules needed to meet the requirements, to reduce drag. The latter implies that there is a maximum value for the drag reduction effect of the polymer, after which the drag reduction effect does not change with the polymer concentration [193]. A typical polymer concentration versus drag reduction curve is shown in Fig. 13(c).

In 1987, the finitely extensible nonlinear elastic–Peterlin (FENE-P) model for polymer studies was proposed and refined to make simulation studies possible [194]. In 1997, Sureshkumar et al. [195] carried out the first simulation studies of polymers with the correct viscoelastic principal equations. The simulation results match well with the results of previous studies that used particle velocimetry and laser Doppler velocimetry equipment. In summary, the experimental equipment used for polymer drag reduction includes pipes [185, 196], rotating equipment such as rheometers [197] and flat plates [198, 199]. In the simulation, most of the studies are conducted by direct numerical simulation, using models such as Oldroyd-B model [200], FENE-P model, etc. The content of the early experimental studies can be borrowed from Virk's study [201], and the subsequent development of the model and the effect of turbulent polymers on the flow field, etc., can be borrowed from the work of Xi [202], Graham [203], and other researchers. In Section 5.2, the drag reduction principle of polymers is specified as a reference for the principle of the drag reduction effect of fish slime.

5.2 Drag reduction principles

Over the past eighty years of research on polymers, researchers have assessed the drag reduction effect of polymers, analyzed the drag reduction factors of polymers, and evaluated the drag reduction mechanism of polymers from experimental, theoretical, and simulation aspects. However, the mechanism of drag reduction has not been fully explored. At present, the more popular theories of polymer drag reduction include viscous theory and elastic theory [152]. Other drag reduction mechanisms are also extended based on these two theories, such as the viscous anisotropy theory and other drag reduction theories [152].

Viscosity theory, mainly proposed and refined by researchers such as Lumley [204] and Ryskin [205], theorizes that changes such as polymer extension in the solvent can greatly affect the viscosity of the solution and that an increase in the viscosity of the solution has the effect of suppressing turbulence fluctuations, reducing the turbulent coherent structure near the wall, and increasing the thickness of the viscous underlayment in the boundary layer, thus realizing the associated drag reduction effect. Ryskin [205] derived the relationship between the increase in effective viscosity and polymer ductility and reported that the effective viscosity is related to the concentration and maximum ductility, verifying Lumley's conjecture.

The elastic theory was mainly proposed and refined by researchers such as Tabor and de Gennes [206], and Sreenivasan and White [207], and the principle is shown in Fig. 13(e). Experimental observations revealed that the polymer remained active at the middle position of the tube, which could not be satisfactorily explained by the viscous theory. Tabor then concluded that the elasticity of the semiductile polymer played an important role in drag reduction. The theory suggests that the drag reduction initiation point exists in large part because the polymer is accumulating elastic energy, which produces a significant drag reduction effect when the energy is close to the near-wall turbulent kinetic energy scale [208]. Owing to the presence of polymers, the turbulent kinetic energy of the fluid is reduced by their influence, reducing the degree of turbulence and decreasing the energy dissipation of the fluid motion, which reduces the fluid drag and the fluid motion noise [202]. In addition, the polymer absorbs the energy of the flow at the wall, increases and releases elastic energy under the action of vortices, and reduces the resistance parameters such as wall shear stresses, thus realizing a reduction in drag [209].

The most significant difference between the two theories is the assumption on which the theory is founded. The viscous theory assumes that the polymer in the solvent is sufficiently ductile to produce a large viscous effect, whereas the elastic theory assumes that this assumption does not hold. In particular, when the drag reduction effect first appears, it is believed that the polymer is only partially extended and the deformation is transient, so the viscous effect is not obvious, while the stored energy has a greater impact on the drag reduction effect. Overall, the two theories are not right or wrong, and their respective theories can explain part of the experimental phenomena; however, for phenomena such as the point of maximum drag reduction rate, both theories fail to explain accurately, and further research and development are needed. For example, from the perspective of dynamic drag reduction framework. Recently, Zhao et al. [210] studied the drag reduction characteristics of poly(allyl methacrylate-co-dimethylaminoethyl methacrylate) (P(AM-DMC)). They find that the polymers are stretched by shear stress, which means that it can increase the viscosity and inhibit the turbulence. Moreover, it can absorb the energy and decrease the energy dissipation. This proves that the two theories mentioned above may have combined effects on drag reduction.

5.3 Summary

The compositional analysis has found that fish mucus contains trace polymers, which play an important role in drag reduction of fish mucus; therefore, researchers have focused on conducting in-depth studies on the drag reduction principles of polymer additives. Polymer additives, as a unique drag reduction method, have the advantages of small starting concentration [185], ease and convenience of use, and economic rationalization, which makes polymer additives more widely used in pipelines. However, polymer additives also have several limitations, such as poor continuity, as shown in Fig. 13(d). With increasing time, the drag reduction effect is gradually weakened, at the same time, the polymer additives change the nature of the fluid, which limits its use on some occasions, and some additives will also pollute the environment. For follow-up research, on one hand, since the

principle of polymer additives has not been fully revealed, the principle of polymer drag reduction can be further explored; on the other hand, the synergistic effect of a variety of polymers and the increase in duration still have room for further research, which can achieve further breakthroughs.

6 Conclusions

Research on drag reduction is crucial because it is a way to save energy and increase efficiency [211–213]. When combined with bionics, it raises the bar even higher and facilitates the discovery of functional surfaces or distinctive materials that have superior drag reduction properties. Based on the principle of bionics, in this paper we systematically describe the structural characteristics of the biological prototypes of the four drag reduction methods, namely, surface structure, superhydrophobic surface, compliant wall, and polymer, as well as the related research contents, which include a variety of biological types; we also demonstrate the drag reduction effects of different methods, and analyze the mechanism behind the drag reduction effects, summarized in Table 1. Naturally, more biological prototypes are worthy of emulation, and subsequent studies can be carried out further. The drag reduction principles of many methods still need to be further studied and proven, and more previously unsolved problems are explained through modern simulation platforms. Second, the combination of multiple methods, such as microstructures and polymer additives [214, 215], microstructures and superhydrophobic surfaces [149], superhydrophobic surfaces and polymer additives [216, 217], can further improve the level and efficiency of drag reduction, and these studies provide ideas and references to further improve the drag reduction rate.

Table 1 Summary of biological prototypes, surface morphology, etc.

Drag reduction method	Biological prototype	Surface morphology	Drag reduction mechanism	Drag reduction rate
Surface structure	Shark [5, 10, 27–30, 32, 34–36, 38–46, 48–51, 78, 126, 218–225]	Denticle	The distance between the leading edge vortex and the epidermis decreases. The effect of flow separation is reduced	3%–10%
		Riblet	Protruding height theory and second vortex theory	8%–10%
	Shrimp [83–86]	Abdominal knobbly structures	Increasing the thickness of the boundary layer. Reducing the velocity gradient. The existence of vortices behind the structure	15%
	Loach [88, 90–93]	Crescent structure	Reduction of turbulent kinetic energy and wall shear stress. Existence of vortices on the leeward side	2%–25%
	Puffer [98, 99, 101–105, 107, 226]	Spinelike bump	A return vortex exists upstream. A rising vortex exists downstream	10%–24%
	Crocodile [108]	Rectangular block structure	Water film theory	6%
	Dung beetle [110–112, 114–117, 227]	Pit and protrusion	Generating low velocity regions between neighboring structures. Reducing energy exchange between the upper and lower flow fields	5%
Superhydrophobic surface	Rice leaf [47, 126, 128, 228]	Micron-scale grooves, nanoscale bumps	Effective slip length theory and substitution of solid–liquid and solid–gas interfaces	5%–90%
	Butterfly wing [126, 128, 220, 228]	Micron-scale scales, nanoscale grooves		
	Lotus [123, 126]	Micrometer scale papillae, nanometer scale waxy layer		
	Water strider [124]	Micron-scale bristles, nanoscale grooves		
Compliant wall	Dolphin [155–159, 162, 165, 169, 173, 220, 229–243]	Compliant surface structure	Delayed transition theory and boundary layer perturbation theory	7%–50%
Polymer additives	Fish mucus [178, 179, 182, 183, 188–190, 225, 226, 244–252]	—	Viscous theory and elastic theory	20%–90%

In summary, bionic interfacial drag reduction technology is anticipated to be a powerful enabler of scientific and technological advancements as well as industrial development across a wide range of industries, including aerospace and transportation [253]. The drag reduction technology with bionic interface can be continuously optimized and improved to achieve environmentally friendly and efficient fluid movement. This will have a positive economic impact and support green development.

Declaration of competing interest

The authors have no competing interests to declare that are relevant to the content of this article. The authors Liran Ma and Jianbin Luo are the Youth Editorial Board Member and Editor-in-Chief of this journal.

References

[1] Li M, Shi W B, Shi J, Wang T, Shi L P, Wang X L. Regulation and control of wet friction of soft materials using surface texturing: A review. *Friction* **11**(3): 333–353 (2023)

[2] Zheng Z J, Guo Z G, Liu W M, Luo J B. Low friction of superslippery and superlubricity: A review. *Friction* **11**(7): 1121–1137 (2023)

[3] Zhang J H, Su Y J, Wu J, Wang H D. Recent advances in ocular lubrication. *Friction* **12**(9): 1929–1954 (2024)

[4] Tian G Z, Fan D L, Feng X M, Zhou H G. Thriving artificial underwater drag-reduction materials inspired from aquatic animals: Progresses and challenges. *RSC Adv* **11**(6): 3399–3428 (2021)

[5] Luo Y H. Recent progress in exploring drag reduction mechanism of real sharkskin surface: A review. *J Mech Med Biol* **15**(3): 1530002 (2015)

[6] Chen D K, Cui X X, Su L, Liu X L, Zhang L W, Chen H W. Research progress and development trend of the drag reduction inspired by fish skin. *Prog Org Coat* **182**: 107613 (2023)

[7] Zhu Y, Yang F C, Guo Z G. Bioinspired surfaces with special microstructures and wettability for drag reduction: Which surface design will be a better choice. *Nanoscale* **13**(6): 3463–3482 (2021)

[8] Tian G Z, Zhang Y S, Feng X M, Hu Y S. Focus on bioinspired textured surfaces toward fluid drag reduction: Recent progresses and challenges. *Adv Eng Mater* **24**(1): 2100696 (2022)

[9] Yu C M, Liu M F, Zhang C H, Yan H, Zhang M H, Wu Q S, Liu M J, Jiang L. Bio-inspired drag reduction: From nature organisms to artificial functional surfaces. *Giant* **2**: 100017 (2020)

[10] Chen D K, Liu Y, Chen H W, Zhang D Y. Bio-inspired drag reduction surface from sharkskin. *Biosurf Biotribol* **4**(2): 39–45 (2018)

[11] Klein J. Nature's lubrication solutions. *Friction* **13**(1): 9440965 (2025)

[12] Wang L Y, Wang C, Wang S Y, Sun G, You B. Design and analysis of micronano scale nested-grooved surface structure for drag reduction based on 'Vortex-Driven Design'. *Eur J Mech B—Fluid* **85**: 335–350 (2021)

[13] Liu G J, Yuan Z C, Qiu Z Z, Feng S W, Xie Y C, Leng D X, Tian X J. A brief review of bio-inspired surface technology and application toward underwater drag reduction. *Ocean Eng* **199**: 106962 (2020)

[14] Gu Y Q, Dai D S, Mou J G, Zheng S H, Wu D H, Wang E. Overview of the technology of bionic surface drag reduction. *J Biomim Biomater Biomed Eng* **23**: 59–66 (2015)

[15] Abdulbari H A, Mahammed H D, Hassan Z B Y. Bio-inspired passive drag reduction techniques: A review. *ChemBioEng Rev* **2**(3): 185–203 (2015)

[16] Yu A H, Fu Y, Xie S Z, Guo Z G, Fu F Y, Liu W M. Biomimetic interfaces for drag reduction: From mechanism to applications. *Friction* **13**(3): 9440900 (2025)

[17] Zheng S H, Liang X, Li J Y, Liu Y Y, Tang J. Drag reduction using bionic groove surface for underwater vehicles. *Front Bioeng Biotech* **11**: 1223691 (2023)

[18] Koeltzsch K, Dinkelacker A, Grundmann R. Flow over convergent and divergent wall riblets. *Exp Fluids* **33**(2): 346–350 (2002)

[19] Ma Q, Yan C, Yan R, Xu X, Wang H. Towards direct superlubricity and superlow wear via amino modification of polyhydroxy alcohol solutions. *Friction* **12**(9): 1980–1990 (2024)

[20] Dong H Y, Cheng M J, Zhang Y J, Wei H, Shi F. Extraordinary drag-reducing effect of a superhydrophobic coating on a macroscopic model ship at high speed. *J Mater Chem A* **1**(19): 5886 (2013)

[21] Song W C, Wang C, Wei Y J, Zhang X S, Wang W. Experimental study of microbubble drag reduction on an axisymmetric body. *Mod Phys Lett B* **32**(3): 1850035 (2018)

[22] Rong W T, Zhang H F, Zhang T J, Mao Z G, Liu X W, Song K G. Drag reduction using lubricant-impregnated anisotropic slippery surfaces inspired by bionic fish scale surfaces containing micro-/nanostructured arrays. *Adv Eng Mater* **23**(1): 2000821 (2021)

[23] Luo Y H, Song W, Wang X D. Water repellent/wetting characteristics of various bio-inspired morphologies and fluid drag reduction testing research. *Micron* **82**: 9–16 (2016)

[24] Sun Y W, Yan X P, Yuan C Q, Bai X Q. Insight into tribological problems of green ship and corresponding research progresses. *Friction* **6**(4): 472–483 (2018)

[25] Zhu M F, Ma L R, Luo J B. *L**—An index for evaluating long range performance of autonomous underwater vehicles (AUVs). *Friction* **12**(10): 2205–2221 (2024)

[26] Luo J B, Zhou X. Superlubricitive engineering—Future industry nearly getting rid of wear and frictional energy consumption. *Friction* **8**(4): 643–665 (2020)

[27] Bechert D, Reif W. On the drag reduction of the shark skin. In: Proceeding of 23rd Aerospace Sciences Meeting, Reno, USA, 1985.

[28] Luo Y H, Xu X, Li D, Song W. Recent developments in fabricating drag reduction surfaces covering biological sharkskin morphology. *Rev Chem Eng* **32**(1): 93–113 (2016)

[29] Feld K, Kolborg A N, Nyborg C M, Salewski M, Steffensen J F, Berg-Sørensen K. Dermal denticles of three slowly swimming shark species: Microscopy and flow visualization. *Biomimetics* **4**(2): 38 (2019)

[30] Ankhelyi M V, Wainwright D K, Lauder G V. Diversity of dermal denticle structure in sharks: Skin surface roughness and three-dimensional morphology. *J Morphol* **279**(8): 1132–1154 (2018)

[31] Dai W, Alkahtani M, Hemmer P R, Liang H. Drag-reduction of 3D printed shark-skin-like surfaces. *Friction* **7**(6): 603–612 (2019)

[32] Du Z Z, Li H Y, Cao Y F, Wan X, Xiang Y L, Lv P Y, Duan H L. Control of flow separation using biomimetic shark scales with fixed tilt angles. *Exp Fluids* **63**(10): 158 (2022)

[33] Bechert D W, Bruse M, Hage W, Meyer R. Fluid mechanics of biological surfaces and their technological application. *Naturwissenschaften* **87**(4): 157–171 (2000)

[34] Ott J, Lazalde M, Gu G X. Algorithmic-driven design of shark denticle bioinspired structures for superior aerodynamic properties. *Bioinspir Biomim* **15**(2): 026001 (2020)

[35] Wen L, Weaver J C, Lauder G V. Biomimetic shark skin: Design, fabrication and hydrodynamic function. *J Exp Biol* **217**(10): 1656–1666 (2014)

[36] Oeffner J, Lauder G V. The hydrodynamic function of shark skin and two biomimetic applications. *J Exp Biol* **215**(Pt 5): 785–795 (2012)

[37] Domel A G, Saadat M, Weaver J C, Haj-Hariri H, Bertoldi K, Lauder G V. Shark skin-inspired designs that improve aerodynamic performance. *J R Soc Interface* **15**(139): 20170828 (2018)

[38] Han X, Zhang D Y, Li X, Li Y Y. Bio-replicated forming of the biomimetic drag-reducing surfaces in large area based on shark skin. *Sci Bull* **53**(10): 1587–1592 (2008)

[39] Zhang D Y, Luo Y H, Li X, Chen H W. Numerical simulation and experimental study of drag-reducing surface of a real shark skin. *J Hydrodyn* **23**(2): 204–211 (2011)

[40] Boomsma A, Sotiropoulos F. Direct numerical simulation of sharkskin denticles in turbulent channel flow. *Phys Fluids* **28**(3): 035106 (2016)

[41] Pu X, Li G J, Huang H L. Preparation, anti-biofouling and drag-reduction properties of a biomimetic shark skin surface. *Biol Open* **5**(4): 389–396 (2016)

[42] Ibrahim M D, Amran S N A, Yunos Y S, Rahman M R A, Mohtar M Z, Wong L K, Zulkharnain A. The study of drag reduction on ships inspired by simplified shark skin imitation. *Appl Bionics Biomech* **2018**(1): 7854321 (2018)

[43] Bhatia D, Zhao Y, Yadav D, Wang J. Drag reduction using biomimetic sharkskin denticles. *Eng Technol Appl Sci* **11**(5): 7665–7672 (2021)

[44] Wilga C D, Lauder G V. Function of the heterocercal tail in sharks: Quantitative wake dynamics during steady horizontal swimming and vertical maneuvering. *J Exp Biol* **205**(16): 2365–2374 (2002)

[45] Wilga C D, Lauder G V. Three-dimensional kinematics and wake structure of the pectoral fins during locomotion in leopard sharks *Triakis semifasciata*. *J Exp Biol* **203**(15): 2261–2278 (2000)

[46] Lang A W, Motta P, Hidalgo P, Westcott M. Bristled shark skin: A microgeometry for boundary layer control. *Bioinspir Biomim* **3**(4): 046005 (2008)

[47] Rossi M. Of vortices and vortical layers: An overview. In: *Vortex Structure and Dynamics*. Maurel A, Petitjeans P, Eds. Berlin (Germany): Springer, 2000: 40–123.

[48] Lang A W, Bradshaw M T, Smith J A, Wheelus J N, Motta P J, Habegger M L, Hueter R E. Movable shark scales act as a passive dynamic micro-roughness to control flow separation. *Bioinspir Biomim* **9**(3): 036017 (2014)

[49] Wen L, Weaver J C, Thornycroft P J M, Lauder G V. Hydrodynamic function of biomimetic shark skin: Effect of denticle pattern and spacing. *Bioinspir Biomim* **10**(6): 066010 (2015)

[50] Patricia F W, Guzman D, Iñigo B, Urtzi I, Maria B J, Manu S.

Morphological characterization and hydrodynamic behavior of shortfin mako shark (isurus oxyrinchus) dorsal fin denticles. *J Bionic Eng* **16**(4): 730–741 (2019)
[51] Guo P M, Zhang K, Yasuda Y, Yang W C, Galipon J, Rival D E. On the influence of biomimetic shark skin in dynamic flow separation. *Bioinspir Biomim* **16**(3): 034001 (2021)
[52] Luo Y H, Yuan L, Li J H, Wang J S. Boundary layer drag reduction research hypotheses derived from bio-inspired surface and recent advanced applications. *Micron* **79**: 59–73 (2015)
[53] Wallace J M, Balint J L. Viscous drag reduction using streamwise-aligned riblets: Survey and new results. In: *Turbulence Management and Relaminarisation*. Berlin (Germany): Springer, 1988: 133–147
[54] Coder D, Walker D, McKelvey D, Enzinger S. Drag reduction with riblets on rowing shells. In: Proceedings of the SNAME 22nd American Towing Tank Conference, St. John's, Newfoundland, Canada, 1989.
[55] Launder B E, Li S. A numerical study of riblet effects on laminar flow through a plane channel. *Appl Sci Res* **46**(3): 271–279 (1989)
[56] Liu K N, Christodoulou C, Riccius O, Joseph D D. Drag reduction in pipes lined with riblets. *AIAA J* **28**(10): 1697–1698 (1990)
[57] Walsh M J. Effect of detailed surface geometry on riblet drag reduction performance. *J Aircr* **27**(6): 572–573 (1990)
[58] Djenidi L, Squire L C, Savill A M. High resolution conformal mesh computations for V, U or L groove riblets in laminar and turbulent boundary layers. In: *Recent Developments in Turbulence Management*. Dordrecht (the Netherlands): Springer, 1991: 65–92.
[59] Nakao S I. Application of V shape riblets to pipe flows. *J Fluids Eng* **113**(4): 587–590 (1991)
[60] Neumann D, Dinkelacker A. Drag measurements on V-grooved surfaces on a body of revolution in axial flow. *Appl Sci Res* **48**(1): 105–114 (1991)
[61] Feng B B, Chen D R, Wang J D, Yang X T. Bionic research on bird feather for drag reduction. *Adv Mech Eng* **7**(2): 849294 (2015)
[62] Chen H W, Rao F G, Zhang D Y, Shang X P. Drag reduction study about bird feather herringbone riblets. *Appl Mech Mater* **461**: 201–205 (2013)
[63] Chen H W, Rao F G, Shang X P, Zhang D Y, Hagiwara I. Biomimetic drag reduction study on herringbone riblets of bird feather. *J Bionic Eng* **10**(3): 341–349 (2013)
[64] Walsh M, Weinstein L. Drag and heat transfer on surfaces with small longitudinal fins. In: Proceedings of the 11th Fluid and PlasmaDynamics Conference, Seattle, USA, 1978.
[65] Walsh M J, Weinstein L M. Drag and heat-transfer characteristics of small longitudinally ribbed surfaces. *AIAA J* **17**(7): 770–771 (1979)
[66] Walsh M J. Drag characteristics of V-groove and transverse curvature riblets. In: Proceedings of the Symposium on Viscous Flow Drag Reduction, Dallas, USA, 1980.
[67] Walsh M. Turbulent boundary layer drag reduction using riblets. In: Proceedings of the 20th Aerospace Sciences Meeting, Orlando, USA, 1982.
[68] Walsh M, Lindemann A. Optimization and application of riblets for turbulent drag reduction. In: Proceedings of the 22nd Aerospace Sciences Meeting, Reno, NV, USA, 1984.
[69] Quass B, Howard F, Weinstein L, Bushnell D. Longitudinal grooves for bluff body drag reduction. *AIAA J* **19**(4): 535–537 (1981)
[70] Gallagher J, Thomas A. Turbulent boundary layer characteristics over streamwise grooves. In: Proceedings of 2nd Applied Aerodynamics Conference, Seattle, WA, USA, 1984.
[71] Bushnell D M, Hefner J N. *Viscous Drag Reduction in Boundary Layers*. Washington DC (USA): the American Institute of Aeronautics and Astronautics Inc., 1990.
[72] Bacher E, Smith C. A combined visualization-anemometry study of the turbulent drag reducing mechanisms of triangular micro-groove surface modifications. In: Proceedings of the Shear Flow Control Conference, Boulder, CO, USA, 1985.
[73] Weiss M H. Drag Reduction in Pipe Flow with Riblets. Ph.D. Thesis. Calgary (Canada): University of Calgary, 1993.
[74] Bechert D W, Bruse M, Hage W, Van Der Hoeven J G T, Hoppe G. Experiments on drag-reducing surfaces and their optimization with an adjustable geometry. *J Fluid Mech* **338**: 59–87 (1997)
[75] García-Mayoral R, Jiménez J. Drag reduction by riblets. *Philos T R Soc A* **369**(1940): 1412–1427 (2011)
[76] García-Mayoral R, Jiménez J. Hydrodynamic stability and breakdown of the viscous regime over riblets. *J Fluid Mech* **678**: 317–347 (2011)
[77] Frohnapfel B, Jovanović J, Delgado A. Experimental investigations of turbulent drag reduction by surface-embedded grooves. *J Fluid Mech* **590**: 107–116 (2007)
[78] Bechert D W, Bruse M, Hage W. Experiments with three-dimensional riblets as an idealized model of shark skin. *Exp Fluids* **28**(5): 403–412 (2000)
[79] Bechert D W, Bartenwerfer M. The viscous flow on surfaces with longitudinal ribs. *J Fluid Mech* **206**: 105–129 (1989)
[80] Sasamori M, Mamori H, Iwamoto K, Murata A. Experimental study on drag-reduction effect due to sinusoidal riblets in turbulent channel flow. *Exp Fluids* **55**(10): 1828 (2014)
[81] West N, Sammut K, Tang Y H. Material selection and manufacturing of riblets for drag reduction: An updated review. *P I Mech Eng L—J Mat* **232**(7): 610–622 (2018)
[82] Mawignon F J, Liu J B, Qin L G, Kouediatouka A N, Ma Z Y, Lv B H, Dong G N. The optimization of biomimetic sharkskin riblet for the adaptation of drag reduction. *Ocean Eng* **275**: 114135 (2023)
[83] Stacey M T, Mead K S, Koehl M A R. Molecule capture by olfactory antennules: Mantis shrimp. *J Math Biol* **44**(1): 1–30 (2002)
[84] Zack T I, Claverie T, Patek S N. Elastic energy storage in the mantis shrimp's fast predatory strike. *J Exp Biol* **212**(24): 4002–4009 (2009)
[85] Rosario M V, Patek S N. Multilevel analysis of elastic morphology: The mantis shrimp's spring. *J Morphol* **276**(9): 1123–1135 (2015)
[86] Gu Y Q, Xia K, Zhang W Q, Mou J G, Wu D H, Liu W, Xu M S, Zhou P J, Ren Y. Airfoil profile surface drag reduction characteristics based on the structure of the mantis shrimp abdominal segment. *Arch Appl Mech* **91**(3): 919–932 (2020)
[87] Sudo S, Tsuyuki K, Ito Y, Ikohagi T. A study on the surface shape of fish scales. *JSME Int J C—Mech Sy* **45**(4): 1100–1105 (2002)
[88] Wu L Y, Jiao Z B, Song Y Q, Ren W T, Niu S C, Han Z W. Water-trapping and drag-reduction effects of fish *Ctenopharyngodon idellus* scales and their simulations. *Sci China Technol Sci* **60**(7): 1111–1117 (2017)
[89] Dou Z L, Wang J D, Chen D R. Bionic research on fish scales for drag reduction. *J Bionic Eng* **9**(4): 457–464 (2012)
[90] Wu L Y, Jiao Z B, Song Y Q, Liu C H, Wang H, Yan Y Y. Experimental investigations on drag-reduction characteristics of bionic surface with water-trapping microstructures of fish scales. *Sci Rep* **8**(1): 12186 (2018)
[91] Wu L Y, Wang H, Song Y Q, Zhang B H, Xu Y, Liu C H, Yan Y Y. Drag reduction mechanism of Paramisgurnus dabryanus loach with self-lubricating and flexible micro-morphology. *Sci Rep* **10**: 12873 (2020)
[92] Wu L Y, Wang J Q, Luo G H, Wang S Q, Qu J W, Fan X G, Liu C H. Study on the drag reduction characteristics of the surface morphology of paramisgurnus dabryanus loach. *Coatings* **11**(11): 1357 (2021)
[93] Wu L Y, Luo G H, He F F, Chen L, Wang S Q, Fan X G. Bionic research on *Paramisgurnus dabryanus* scales for drag reduction. *RSC Adv* **12**(34): 22226–22235 (2022)
[94] Monfared Mosghani M, Ali Alidoostan M, Binesh A. Numerical analysis of drag reduction of fish scales inspired Ctenoid-shape microstructured surfaces. *Chem Eng Commun* **210**(6): 970–985 (2023)
[95] Wang Y H, Zhang Z B, Xu J K, Yu H D. One-step method using

laser for large-scale preparation of bionic superhydrophobic & drag-reducing fish-scale surface. *Surf Coat Tech* **409**: 126801 (2021)
[96] Sun T L, Lyu Y S, Li X S. Drag reduction analysis of structured topological fish scale surface. Proceedings of the 3rd International Conference on Mechanical, Electronics, and Electrical and Automation Control (METMS 2023), Hangzhou, China, 2023.
[97] Yan H, Xie T Z, Wang F, Zeng Y S, Ai J Q. Effect of biomimetic fish scale structure on the drag reduction performance of Clark-Y hydrofoil. *P I Mech Eng M—J Eng* **238**(4): 763–777 (2024)
[98] Zhou H G, Shen D, Tian G Z, Cui J, Jia C F. Biomechanical characteristics of puffer skin for flexible surface drag reduction. *Mech Adv Mater Struct* **28**(11): 1194–1200 (2021)
[99] Zhou H G, Liu C Q, Tian G Z, Feng X M, Jia C F. Research on the drag reduction property of puffer (*Takifugu flavidus*) spinal nonsmooth structure surface. *Microsc Res Tech* **83**(7): 795–803 (2020)
[100] Su F Y, Bushong E A, Deerinck T J, Seo K, Herrera S, Graeve O A, Kisailus D, Lubarda V A, McKittrick J. Spines of the porcupine fish: Structure, composition, and mechanical properties. *J Mech Behav Biomed Mater* **73**: 38–49 (2017)
[101] Fan D L, Feng X M, Tian G Z, Zhang Y S. Experimental investigations of the turbulent boundary layer for biomimetic protrusive surfaces inspired by pufferfish skin: Effects of spinal density and diameter. *Langmuir* **37**(40): 11804–11817 (2021)
[102] Feng X M, Jia C F, Fan D L, Hu Y S, Tian G Z. Numerical analysis of drag reduction characteristics of biomimetic puffer skin: Effect of spinal arrangement. *AIP Adv* **11**(6): 065223 (2021)
[103] Zhou H G, Zhu Y S, Tian G Z, Feng X M, Zhang Y S. Experimental investigations of the turbulent boundary layer for biomimetic surface with spine-covered protrusion inspired by pufferfish skin. *Arab J Sci Eng* **46**(3): 2865–2875 (2021)
[104] Zhou H G, Jia C F, Tian G Z, Feng X M, Fan D L. Numerical analysis of drag reduction characteristics of biomimetic puffer skin: Effect of spinal height and tilt angle. *J Nanosci Nanotechnol* **21**(9): 4615–4624 (2021)
[105] Feng X M, Fan D L, Tian G Z, Zhang Y S. Coupled bionic drag-reducing surface covered by conical protrusions and elastic layer inspired from pufferfish skin. *ACS Appl Mater Inter* **14**(28): 32747–32760 (2022)
[106] Tian G Z, Shi J, Hu Y S, Zhou H G, Feng X M. Numerical-experimental study on the influence of the biomimetic spine-covered protrusions (BSCPs) structure on the base pressure and near-wake flow of underwater vehicles. *Arab J Sci Eng* **47**(6): 6821–6835 (2022)
[107] Zhang Y S, Fan D L, Feng X M, Hu Y S, Shi J, Tian G Z. Drag reduction performance and mechanism of flexible conical microstructure film inspired by pufferfish epidermis. *Ocean Eng* **271**: 113760 (2023)
[108] Yan G Q, Tian P, Mo J S, Xie H, Wei H L. Low-velocity resistance distortion and bionic drag reduction for ship-type paddy field machinery. *Int J Agric Biol Eng* **13**(2): 7–14 (2020)
[109] Fountaine E R. Investigations into the mechanism of soil adhesion. *J Soil Sci* **5**(2): 251–263 (1954)
[110] Tong J, Sun J Y, Chen D H, Zhang S J. Geometrical features and wettability of dung beetles and potential biomimetic engineering applications in tillage implements. *Soil Tillage Res* **80**(1–2): 1–12 (2005)
[111] Li J, Cui Z, Ren L, Sun J, Yan Y Y. Reduction of sliding resistance between clay and bionics plates. In: *Design and Nature II*. Collins M W, Brebbia C A, Eds. Southampton (UK): WIT Press, 2004.
[112] Kui H L, Wang P X, Li J, Ni W X. Biomimetic design of diesel engine inlet. In: Proceedings of the 2011 International Conference on Transportation, Mechanical, and Electrical Engineering (TMEE), Changchun, China, 2011: 747–750.
[113] An Y Y, Wei W, Li S S, Liu C, Meng X L, Yan Q D. Research on the mechanism of drag reduction and efficiency improvement of hydraulic retarders with bionic non-smooth surface spoilers. *Eng Appl Comput Fluid Mech* **14**(1): 447–461 (2020)
[114] Sun J Y, Wang Y M, Zhang S J, Ma Y H, Tong J, Zhang Z J. The mechanism of resistance-reducing/anti-adhesion and its application on biomimetic disc furrow opener. *Math Biosci Eng* **17**(5): 4657–4677 (2020)
[115] Tan Y, Liu S, Ma S C. Application of Bionics Engineering in Innovative design of Agricultural Machinery. In: Proceedings of the 2020 ASABE Annual International Virtual Meeting, 2020.
[116] Dai C, Guo C, Ge Z P, Liu H L, Dong L. Study on drag and noise reduction of bionic blade of centrifugal pump and mechanism. *J Bionic Eng* **18**(2): 428–440 (2021)
[117] Cui B L, Wang Z, Zhang Y B, Han X T. Drag and pressure pulsation reduction of a low-specific-speed centrifugal pump by employing bionic structure. *Mod Phys Lett B* **36**(7): 2150611 (2022)
[118] Wang Y Q, Weng D, Wei Y J, Ma Y, Chen L, Wang J D. Aerodynamic drag reduction on speed skating helmet by surface structures. *Appl Sci* **13**(1): 130 (2023)
[119] Zhu Z Y, Li J, Peng H, Liu D R. Nature-inspired structures applied in heat transfer enhancement and drag reduction. *Micromachines* **12**(6): 656 (2021)
[120] Young T. III. An essay on the cohesion of fluids. *Phil Trans R Soc* **95**: 65–87 (1805)
[121] Luo Y H, Zhang D Y, Liu Y F. Recent drag reduction developments derived from different biological functional surfaces: A review. *J Mech Med Biol* **16**(2): 1630001 (2016)
[122] Bhushan B, Jung Y C. Natural and biomimetic artificial surfaces for superhydrophobicity, self-cleaning, low adhesion, and drag reduction. *Prog Mater Sci* **56**(1): 1–108 (2011)
[123] Barthlott W, Neinhuis C. Purity of the sacred lotus, or escape from contamination in biological surfaces. *Planta* **202**(1): 1–8 (1997)
[124] Gao X F, Jiang L. Water-repellent legs of water striders. *Nature* **432** (7013): 36 (2004)
[125] Liravi M, Pakzad H, Moosavi A, Nouri-Borujerdi A. A comprehensive review on recent advances in superhydrophobic surfaces and their applications for drag reduction. *Prog Org Coat* **140**: 105537 (2020)
[126] Bixler G D, Bhushan B. Bioinspired rice leaf and butterfly wing surface structures combining shark skin and lotus effects. *Soft Matter* **8**(44): 11271 (2012)
[127] Gao X, Yan X, Yao X, Xu L, Zhang K, Zhang J, Yang B, Jiang L. The dry-style antifogging properties of mosquito compound eyes and artificial analogues prepared by soft lithography. *Adv Mater* **19**(17): 2213–2217 (2007)
[128] Bixler G D, Bhushan B. Rice- and butterfly-wing effect inspired self-cleaning and low drag micro/nanopatterned surfaces in water, oil, and air flow. *Nanoscale* **6**(1): 76–96 (2014)
[129] Neinhuis C, Barthlott W. Characterization and distribution of water-repellent, self-cleaning plant surfaces. *Ann Bot* **79**(6): 667–677 (1997)
[130] Liu X J, Liang Y M, Zhou F, Liu W M. Extreme wettability and tunable adhesion: Biomimicking beyond nature. *Soft Matter* **8**(7): 2070–2086 (2012)
[131] Kim J, Kim C J. Nanostructured surfaces for dramatic reduction of flow resistance in droplet-based microfluidics. In: Proceedings of the MEMS IEEE International Conference, 15th IEEE International Conference on Micro Electro Mechanical System, Las Vegas, USA, 2002: 479–482.
[132] Henoch C, Krupenkin T, Kolodner P, Taylor J, Hodes M, Lyons A, Peguero C, Breuer K. Turbulent drag reduction using superhydrophobic surfaces. In: Proceedings of the 3rd AIAA Flow Control Conference, San Francisco, USA, 2006.
[133] Daniello R J, Waterhouse N E, Rothstein J P. Drag reduction in turbulent flows over superhydrophobic surfaces. *Phys Fluids* **21**(8): 085103 (2009)
[134] Du P, Wen J, Zhang Z Z, Song D, Ouahsine A, Hu H B.

Maintenance of air layer and drag reduction on superhydrophobic surface. *Ocean Eng* **130**: 328–335 (2017)
[135] Taghvaei E, Moosavi A, Nouri-Borujerdi A, Daeian M A, Vafaeinejad S. Superhydrophobic surfaces with a dual-layer micro- and nanoparticle coating for drag reduction. *Energy* **125**: 1–10 (2017)
[136] Monfared M, Alidoostan M A, Saranjam B. Experimental study on the friction drag reduction of superhydrophobic surfaces in closed channel flow. *J Appl Fluid Mech* **12**(1): 69–76 (2019)
[137] Hu J G, Yao Z H. Drag reduction of turbulent boundary layer over sawtooth riblet surface with superhydrophobic coat. *Phys Fluids* **35**(1): 015104 (2023)
[138] Min T, Kim J. Effects of hydrophobic surface on skin-friction drag. *Phys Fluids* **16**(7): L55–L58 (2004)
[139] Fukagata K, Kasagi N, Koumoutsakos P. A theoretical prediction of friction drag reduction in turbulent flow by superhydrophobic surfaces. *Phys Fluids* **18**(5): 051703 (2006)
[140] Nouri N M, Sekhavat S, Mofidi A. Drag reduction in a turbulent channel flow with hydrophobic wall. *J Hydrodyn* **24**(3): 458–466 (2012)
[141] Nouri N M, Bakhsh M S, Sekhavat S. Analysis of shear rate effects on drag reduction in turbulent channel flow with superhydrophobic wall. *J Hydrodyn* **25**(6): 944–953 (2013)
[142] Park H, Park H, Kim J. A numerical study of the effects of superhydrophobic surface on skin-friction drag in turbulent channel flow. *Phys Fluids* **25**(11): 110815 (2013)
[143] Cheng Y P, Xu J L, Sui Y. Numerical study on drag reduction and heat transfer enhancement in microchannels with superhydrophobic surfaces for electronic cooling. *Appl Therm Eng* **88**: 71–81 (2015)
[144] Jung T, Choi H, Kim J. Effects of the air layer of an idealized superhydrophobic surface on the slip length and skin-friction drag. *J Fluid Mech* **790**: R1 (2016)
[145] Li C X, Zhang S, Xue Q X, Ye X M. Simulation of drag reduction in superhydrophobic microchannels based on parabolic gas–liquid interfaces. *Phys Fluids* **28**(10): 102004 (2016)
[146] Im H J, Lee J H. Comparison of superhydrophobic drag reduction between turbulent pipe and channel flows. *Phys Fluids* **29**(9): 095101 (2017)
[147] Mollicone J P, Battista F, Gualtieri P, Casciola C M. Superhydrophobic surfaces to reduce form drag in turbulent separated flows. *AIP Adv* **12**(7): 075003 (2022)
[148] Nguyen H T, Chang K, Lee S W, Ryu J, Kim M. Numerical prediction of turbulent drag reduction with different solid fractions and distribution shapes over superhydrophobic surfaces. *Energies* **15**(18): 6645 (2022)
[149] Safari A, Saidi M H, Salavatidezfouli S, Yao S H. Numerical investigation of the drag reduction effect in turbulent channel flow by superhydrophobic grooved surfaces. *Flow* **3**: E27 (2023)
[150] Park H, Choi C H, Kim C J. Superhydrophobic drag reduction in turbulent flows: A critical review. *Exp Fluids* **62**(11): 229 (2021)
[151] Lee C, Choi C H, Kim C J. Superhydrophobic drag reduction in laminar flows: A critical review. *Exp Fluids* **57**(12): 176 (2016)
[152] Liu M, Ma L R. Drag reduction methods at solid-liquid interfaces. *Friction* **10**(4): 491–515 (2022)
[153] Wang J D, Wang B, Chen D R. Underwater drag reduction by gas. *Friction* **2**(4): 295–309 (2014)
[154] Gray J. Studies in animal locomotion. *J Exp Biol* **13**(2): 192–199 (1936)
[155] Pavlov V, Riedeberger D, Rist U, Siebert U. Analysis of the relation between skin morphology and local flow conditions for a fast-swimming dolphin. In: *Nature-Inspired Fluid Mechanics*. Berlin (Germany): Springer, 2012: 239–253.
[156] Fish F E. The myth and reality of gray's paradox: Implication of dolphin drag reduction for technology. *Bioinspir Biomim* **1**(2): R17–R25 (2006)
[157] Fish F E, Hui C A. Dolphin swimming—A review. *Mammal Rev* **21**(4): 181–195 (1991)
[158] Wainwright D K, Fish F E, Ingersoll S, Williams T M, St Leger J, Smits A J, Lauder G V. How smooth is a dolphin? The ridged skin of odontocetes. *Biol Lett* **15**(7): 20190103 (2019)
[159] Cozzi B, Huggenberger S, Oelschläger H A. *Anatomy of Dolphins: Insights into Body Structure And Function*. New York (USA): Academic Press, 2016.
[160] Fukagata K, Kern S, Chatelain P, Koumoutsakos P, Kasagi N. Evolutionary optimization of an anisotropic compliant surface for turbulent friction drag reduction. *J Turbul* **9**: N35 (2008)
[161] Li L C, Liu B, Hao H L, Li L Y, Zeng Z X. Investigation of the drag reduction performance of bionic flexible coating. *Phys Fluids* **32**(8): 084103 (2020)
[162] Lang A W, Jones E M, Afroz F. Separation control over a grooved surface inspired by dolphin skin. *Bioinspir Biomim* **12**(2): 026005 (2017)
[163] Kramer M O. Boundary-layer stabilization by distributed damping. *J Aerosp Sci* **27**(1): 69 (1960)
[164] Kramer M O. Boundary layer stabilization by distributed damping. *Nav Eng J* **74**(2): 341–348 (1962)
[165] Kramer M O. The dolphins' secret. *J Am Soc Nav Eng* **73**(1): 103–108 (1961)
[166] Gad-el-Hak M. Compliant coatings for drag reduction. *Prog Aerosp Sci* **38**(1): 77–99 (2002)
[167] Carpenter P W, Lucey A D, Dixon A E. The optimisation of compliant walls for drag reduction. *Recent Developments in Turbulence Management*. Dordrecht (the Netherlands): Springer, 1991: 195–221
[168] Choi K S, Yang X, Clayton B R, Glover E J, Atlar M, Semenov B N, Kulik V M. Turbulent drag reduction using compliant surfaces. *P Roy Soc Lond A Mat* **453**(1965): 2229–2240 (1997)
[169] Nagamine H, Yamahata K, Hagiwara Y, Matsubara R. Turbulence modification by compliant skin and strata-corneas desquamation of a swimming dolphin. *J Turbulence* **5**: N18 (2004)
[170] Matsumura R, Koyama S, Hagiwara Y. Turbulent drag reduction by wall deformation synchronized with flow acceleration. In: Proceedings of the IUTAM Symposium on Computational Physics and New Perspectives in Turbulence, Nagoya, Japan, 2008: 385–390
[171] Lee I, Kulik V M, Boiko A V, Chun H H. Experimental investigation of drag reducing mechanism of compliant coating with optimal viscoelastic properties. In: Proceeding of the 6th International Symposium on Turbulence and Shear Flow Phenomena, Seoul, Republic of Korea, 2009.
[172] Boiko A V, Kulik V M, Chun H H, Lee I. Verification of drag-reduction capabilities of stiff compliant coatings in air flow at moderate speeds. *Int J Nav Archit Ocean Eng* **3**(4): 242–253 (2011)
[173] Shang Y G, Jin E, Ke Q P, Han Y M, Gao Z H, Tian L M. Efficiency improvement of centrifugal pump with function surface imitating dolphin skin structure. *Trans Chin Soc Agric Eng* **32**(7): 72–78 (2016) (in Chinese)
[174] Schrader L U. Passive drag reduction via bionic hull coatings. *J Ship Res* **63**(3): 206–218 (2019)
[175] Chen L, Liu S G, Zhao D, Guo H T, Wei J D, Liu Y X. Stability and drag reduction in turbulent flow of skin with quasi-periodic elastic supports. *P I Mech Eng M—J Eng* **236**(4): 1057–1068 (2022)
[176] Gu Y Q, Dai D S, Mou J G, Zheng S H, Jiang L F, Sun Z Z, Wang E. Overview of the mechanisms of drag reduction by means of flexible surfaces. *J Biomim Biomater Biomed Eng* **23**: 18–23 (2015)
[177] Yan M H, Gu Y Q, Ma L B, Tang J X, He C D, Zhang J J, Mou J G. Slime-groove drag reduction characteristics and mechanism of marine biomimetic surface. *Appl Bionics Biomech* **2022**(1): 4485365 (2022)
[178] Litt M. Mucus rheology. relevance to mucociliary clearance. *Arch Intern Med* **126**(3): 417–423 (1970)
[179] Litt M. Flow behavior of mucus. *Ann Otol Rhinol Laryngol* **80**(3): 330–335 (1971)

[180] Hoyt J W. Hydrodynamic drag reduction due to fish slimes. In: *Swimming and Flying in Nature*. Berlin (Germany): Springer, 1975: 653–672
[181] Rosen M W, Cornford N E. Fluid friction of fish slimes. *Nature* **234**(5323): 49–51 (1971)
[182] Daniel T L. Fish mucus: *In situ* measurements of polymer drag reduction. *Biol Bull* **160**(3): 376–382 (1981)
[183] Parrish J K, Kroen W K. Sloughed mucus and drag-reduction in a school of Atlantic silversides, Menidia menidia. *Mar Biol* **97**(2): 165–169 (1988)
[184] Fudge D S, Levy N, Chiu S, Gosline J M. Composition, morphology and mechanics of hagfish slime. *J Exp Biol* **208**(24): 4613–4625 (2005)
[185] Quan Q, Wang S X, Wang L, Shi Y, Xie J, Wang X D, Wang S W. Experimental study on the effect of high-molecular polymer as drag reducer on drag reduction rate of pipe flow. *J Petrol Sci Eng* **178**: 852–856 (2019)
[186] Yanuar Y, Talahatu M A, Sunaryo S, Warjito W. Drag reduction by biopolymer of monepterus albus slime on ship model wall. *Jurnal Mekanikal* **32**(1): 96–107 (2011)
[187] Yanuar Y, Gunawan G, Talahatu M A, Indrawati R T, Jamaluddin A. Resistance reduction on trimaran ship model by biopolymer of eel slime. *J Nav Arch Mar Engg* **12**(2): 95–102 (2015)
[188] Wood M. Biomimetic research of fish mucus and cargo ships. *J Stud Res* **11**(3): 1–5 (2022)
[189] Tian F B. Hydrodynamic effects of mucus on swimming performance of an undulatory foil by using the DSD/SST method. *Comput Mech* **65**(3): 751–761 (2020)
[190] Zhang K S, Ma C F, Zhang B C, Zhao B, Wang Q. Numerical simulation study on bionic mucus drag reduction of underwater vehicle. *Inter J Fluid Mech Res* **47**(4): 371–385 (2020)
[191] Toms B A. Some observations on the flow of linear polymersolutions through straight tubes at large Reynolds numbers. *Proc of In Cong On Rheology* **135**: 135–141 (1948)
[192] Virk P S, Merrill E W, Mickley H S, Smith K A, Mollo-Christensen E L. The Toms phenomenon: Turbulent pipe flow of dilute polymer solutions. *J Fluid Mech* **30**(2): 305–328 (1967)
[193] White C M, Mungal M G. Mechanics and prediction of turbulent drag reduction with polymer additives. *Annu Rev Fluid Mech* **40**: 235–256 (2008)
[194] Bird R B, Armstrong R C, Hassager O. *Dynamics of Polymeric Liquids. Vol. 1: Fluid Mechanics*, 2nd edn. New York (USA): Wiley-Interscience, 1987.
[195] Sureshkumar R, Beris A N, Handler R A. Direct numerical simulation of the turbulent channel flow of a polymer solution. *Phys Fluids* **9**(3): 743–755 (1997)
[196] Mohammadtabar M, Sanders R S, Ghaemi S. Viscoelastic properties of flexible and rigid polymers for turbulent drag reduction. *J Non-Newton Fluid Mech* **283**: 104347 (2020)
[197] Peyser P, Little R C. The drag reduction of dilute polymer solutions as a function of solvent power, viscosity, and temperature. *J Appl Polym Sci* **15**(11): 2623–2637 (1971)
[198] Larson R G. Analysis of polymer turbulent drag reduction in flow past a flat plate. *J Non-Newton Fluid Mech* **111**(2–3): 229–250 (2003)
[199] Petrie H L, Deutsch S, Brungart T A, Fontaine A A. Polymer drag reduction with surface roughness in flat-plate turbulent boundary layer flow. *Exp Fluids* **35**(1): 8–23 (2003)
[200] Min T, Yul Yoo J, Choi H, Joseph D D. Drag reduction by polymer additives in a turbulent channel flow. *J Fluid Mech* **486**: 213–238 (2003)
[201] Virk P S. Drag reduction fundamentals. *AlChE J* **21**(4): 625–656 (1975)
[202] Xi L. Turbulent drag reduction by polymer additives: Fundamentals and recent advances. *Phys Fluids* **31**(12): 121302 (2019)
[203] Graham M D. Drag reduction in turbulent flow of polymer solutions. *Rheol Rev* **2**(2): 143–170 (2004)
[204] Lumley J L. Drag reduction by additives. *Annu Rev Fluid Mech* **1**: 367–384 (1969)
[205] Ryskin G. Turbulent drag reduction by polymers: A quantitative theory. *Phys Rev Lett* **59**(18): 2059–2062 (1987)
[206] Tabor M, de Gennes P G. A cascade theory of drag reduction. *Europhys Lett* **2**(7): 519–522 (1986)
[207] Sreenivasan K R, White C M. The onset of drag reduction by dilute polymer additives, and the maximum drag reduction asymptote. *J Fluid Mech* **409**: 149–164 (2000)
[208] Kulmatova D. Turbulent drag reduction by additives. Ph. D. Thesis. Amsterdam (the Netherlands): Universiteit van Amsterdam, 2013.
[209] Han W, Dong Y, Choi H. Applications of water-soluble polymers in turbulent drag reduction. *Processes* **5**(2): 24 (2017)
[210] Zhao M W, Liu S C, Dai C L, Yan R Q, Li Y, Liu P. Development and drag reduction behaviors of a water-in-water emulsion polymer drag reducer. *ACS Appl Polym Mater* **5**(5): 3707–3716 (2023)
[211] Zhou Z R. Tribology in China. *Friction* **13**(1): 9440994 (2025)
[212] Xin L, Li H, Gao J, Wang Z W, Zhou K J, Yu S R. Large-scale fabrication of decoupling coatings with promising robustness and superhydrophobicity for antifouling, drag reduction, and organic photodegradation. *Friction* **11**(5): 716–736 (2023)
[213] Meng Y G, Xu J, Jin Z M, Prakash B, Hu Y Z. A review of recent advances in tribology. *Friction* **8**(2): 221–300 (2020)
[214] Zhang K, Ma C, Zhang J, Zhang B, Zhao B. Drag reduction characteristics of bionic structure composed of grooves and mucous membrane acting on turbulent boundary layer. *J Appl Fluid Mech* **15**(1): 283–292 (2021)
[215] Koury E, Virk P S. Drag reduction by polymer solutions in a riblet-lined pipe. *Appl Sci Res* **54**(4): 323–347 (1995)
[216] Kouser T, Xiong Y L, Yang D. Contribution of superhydrophobic surfaces and polymer additives to drag reduction. *ChemBioEng Rev* **8**(4): 337–356 (2021)
[217] Rajappan A, McKinley G H. Cooperative drag reduction in turbulent flows using polymer additives and superhydrophobic walls. *Phys Rev Fluids* **5**(11): 114601 (2020)
[218] Chen H W, Zhang X, Che D, Zhang D Y, Li X, Li Y Y. Synthetic effect of vivid shark skin and polymer additive on drag reduction reinforcement. *Adv Mech Eng* **6**: 425701 (2014)
[219] Lang A, Afroz F, Motta P, Wilroy J, Wahidi R, Elliott C, Habegger M L. Sharks, dolphins and butterflies: Micro-sized surfaces have macro effects. In: Proceedings of the ASME 2017 Fluids Engineering Division Summer Meeting, Waikoloa, Hawaii, USA, 2017.
[220] Ghimire A, Dahl R B, Shen S F, Chen P Y. Shark skin denticles: From morphological diversity to multi-functional adaptations and applications. *Adv Funct Mater* **34**(35): 2307121 (2024)
[221] Jo W, Kang H S, Choi J, Jung J, Hyun J, Kwon J, Kim I, Lee H, Kim H T. Light-designed shark skin-mimetic surfaces. *Nano Lett* **21**(13): 5500–5507 (2021)
[222] Luo Y H, Liu Y F, Anderson J, Li X, Li Y Y. Improvement of water-repellent and hydrodynamic drag reduction properties on bio-inspired surface and exploring sharkskin effect mechanism. *Appl Phys A* **120**(1): 369–377 (2015)
[223] Tanvir Ahmmed K M, Montagut J, Kietzig A M. Drag on superhydrophobic sharkskin inspired surface in a closed channel turbulent flow. *Can J Chem Eng* **95**(10): 1934–1942 (2017)
[224] Liu Y B, Gu H M, Jia Y, Liu J, Zhang H, Wang R M, Zhang B L, Zhang H P, Zhang Q Y. Design and preparation of biomimetic polydimethylsiloxane (PDMS) films with superhydrophobic, self-healing and drag reduction properties via replication of shark skin and SI-ATRP. *Chem Eng J* **356**: 318–328 (2019)
[225] Luo Y H, Zhang D Y, Liu Y F, Li Y Y, Ng E Y K. Chemical, mechanical and hydrodynamic properties research on composite drag reduction surface based on biological sharkskin morphology and mucus nanolong chain. *J Mech Med Biol* **15**(5): 1550084 (2015)
[226] Zhang Y S, Feng X M, Tian G Z, Jia C F. Rheological properties and

drag reduction performance of puffer epidermal mucus. *ACS Biomater Sci Eng* **8**(2): 460–469 (2022)
[227] Cui Y Z, Zheng M L, Zhang W, Wang B, Zhang L. Study of dry sliding friction and wear behavior of bionic surface of hardened steel. *Mat Express* **9**(6): 535–544 (2019)
[228] Bixler G D, Bhushan B. Fluid drag reduction and efficient self-cleaning with rice leaf and butterfly wing bioinspired surfaces. *Nanoscale* **5**(17): 7685 (2013)
[229] Nagamine H, Taki A, Murata T, Hagiwara Y, Matsubara R. Turbulence control by compliant skin and strata-corneas desquamation of a swimming dolphin. In: Proceedings of the 3rd Symposium on Turbulence and Shear Flow Phenomena, Sendai, Japan, 2003.
[230] Cohen R C Z, Cleary P W, Mason B R. Simulations of dolphin kick swimming using smoothed particle hydrodynamics. *Hum Mov Sci* **31**(3): 604–619 (2012)
[231] Fish F E. Power output and propulsive efficiency of swimming bottlenose dolphins (*Tursiops truncatus*). *J Exp Biol* **185**(1): 179–193 (1993)
[232] Tanaka H, Li G, Uchida Y, Nakamura M, Ikeda T, Liu H. Measurement of time-varying kinematics of a dolphin in burst accelerating swimming. *PLoS One* **14**(1): e0210860 (2019)
[233] Fish F E, Legac P, Williams T M, Wei T. Measurement of hydrodynamic force generation by swimming dolphins using bubble DPIV. *J Exp Biol* **217**(2): 252–260 (2014)
[234] Goldin N, King R. Learning from dolphin skin–drag reduction by active delay of transition: Flow control by distributed wall actuation. In: *Nature-Inspired Fluid Mechanics*. Berlin (Germany): Springer, 2012: 207–222.
[235] Carpenter P W. Hydrodynamics of dolphin skin and other compliant surfaces. In: *Flow Phenomena in Nature*. Southampton (UK): WIT Press, 2006: 447–456.
[236] Alekseeva T E, Semenov B N. Hydrodynamic drag of the dolphin. *J Appl Mech Tech Phys* **12**(2): 326–329 (1971)
[237] Prabu T, Firthouse A, Baranitharan A M. Hydrodynamic analysis of a flopping NACA0012 hydrofoil and dolphin fish-like model. *J Appl Fluid Mech* **17**(4): 889–899 (2024)
[238] Yuan Y, Ding Z Y, Yu Z X, Zhang Z G. Evaluation of dolphin swimming speed and thrust based on CFD. In: Proceedings of the 12th ISOPE Pacific/Asia Offshore Mechanics Symposium, Gold Coast, Australia, 2016.
[239] Lisi A G. Drag reduction over dolphin skin via the pondermotive forcing of vortex filaments. San Diego (USA): University of California, 1999.
[240] Pavlov V V. Dolphin skin as a natural anisotropic compliant wall. *Bioinspir Biomim* **1**(2): 31–40 (2006)
[241] Zhang H, Yoshitake N, Hagiwara Y. Changes in drag acting on an angled wavy siliconrubber plate as a model of the skin folds of a swimming dolphin. In: *Bio-mechanisms of Swimming and Flying*. Tokyo (Japan): Springer, 2008: 91–102.
[242] Kramer D M O. Boundary layer control by "artificial dolphin coating". *Nav Eng J* **89**(5): 41–45 (1977)
[243] Fitzgerald E R, Fitzgerald J W. Blubber and compliant coatings for drag reduction in fluids III: viscoelastic properties of dolphin blubber matched by a gel-foam composite. In: Proceedings of the 3rd International Conference on Intelligent Materials and 3rd European Conference on Smart Structures and Materials, Lyon, France, 1996.
[244] Huang S X. Viscoelastic characterization of the mucus from the skin of loach. *Korea Aust Rheol J* **33**(1): 1–9 (2021)
[245] Lai S K, Wang Y Y, Wirtz D, Hanes J. Micro- and macrorheology of mucus. *Adv Drug Deliv Rev* **61**(2): 86–100 (2009)
[246] Zhang Y S, Zhang K Z, Zhang Y T, Zhang J. The mechanism of drag reduction performance depending on the secretion rate of biomimetic mucus for a bio-inspired surface. *Ocean Eng* **310**(Part 1): 118594 (2024)
[247] Zhang D G, Chen Y X, Ma Y H, Guo L, Sun J Y, Tong J. Earthworm epidermal mucus: Rheological behavior reveals drag-reducing characteristics in soil. *Soil Tillage Res* **158**: 57–66 (2016)
[248] Bernadsky G, Rosenberg E. Drag-reducing properties of bacteria from the skin mucus of the cornetfish (*Fistularia commersonii*). *Microb Ecol* **24**(1): 63–76 (1992)
[249] Bernadsky G, Sar N, Rosenberg E. Drag reduction of fish skin mucus: Relationship to mode of swimming and size. *J Fish Biol* **42**(5): 797–800 (1993)
[250] Zhao P F, Li X, Luo Z J, Zhai Q H, Tian Y, Zhang K S, Guo H. A bio-inspired drag reduction method of bionic fish skin mucus structure. *Micromachines* **15**(3): 364 (2024)
[251] Cone R A. Barrier properties of mucus. *Adv Drug Deliv Rev* **61**(2): 75–85 (2009)
[252] Ling S C, Ling T Y J. Anomalous drag-reducing phenomenon at a water/fish-mucus or polymer interface. *J Fluid Mech* **65**(3): 499–512 (1974)
[253] Guo L Y, Liu Y, Ma L R, Luo J B. A review of drag reduction technology inspired from biomimetic surfaces and functions. *Friction* **13**(3): 9440876 (2025)

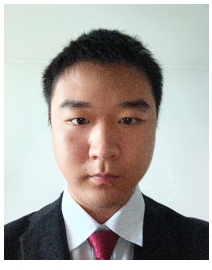

Yiwei Hu obtained his bachelor degree in 2022 from Tsinghua University, China. He subsequently became a Ph.D. candidate under the supervision of Prof. Jianbin Luo at the State Key Laboratory of Tribology in Advanced Equipment (SKLT), Tsinghua University. His research interests include drag reactions via microstructures or other methods.

Yukai Sun received his Ph.D. degree in 2023 from the School of Precision Instrument and Opto-Electronics Engineering at Tianjin University, China. He is now working as a postdoctoral fellow in the SKLT at Tsinghua University, China. His research areas include drag reduction, solid–liquid interface behaviors, and microfluidics.

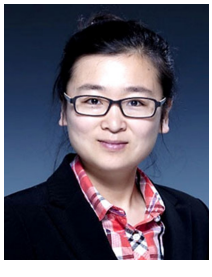

Liran Ma received her Ph.D. degree in 2010 from the Department of Precision Instrument and Mechanology at Tsinghua University, China. Following a postdoctoral period at the Weizmann Institute of Science in Israel, she is now working as an associate professor at the SKLT, Tsinghua University, China. She was elected the Young Chang Jiang Scholar in 2015. Her current research interests are tribology and surface & interface science.

Jianbin Luo obtained his bachelor degree in 1982 from Northeastern University, China. He continued his studies at metal working at Xi'an University of Architecture and Technology, China. He received his M.Eng. degree in 1988. In 1994, he received his Ph.D. degree in mechanical design and theory from Tsinghua University, China and then joined the faculty of Tsinghua University. His research focuses on thin film lubrication, superlubricity, and tribology in nanomanufacturing.